Title: Multi-task machine learning reveals the neuroanatomy fingerprint of mental processing

Authors: Zifan Wang[1,2], Yuzhong Chen[1], Wei Mao[1], Zhenxiang Xiao[1], Guannan Cao[3], Paule-J Toussaint[2], Weitong Guo[1], Boyu Zhao[1], Hailin Sun[1], Tuo Zhang[3], Alan C Evans[2*], and Xi Jiang[1]*

Affiliations:

[1]The Clinical Hospital of Chengdu Brain Science Institute, MOE Key Laboratory for NeuroInformation, School of Life Science and Technology, University of Electronic Science and Technology of China, Chengdu, 611731, China

[2]Montreal Neurological Institute, McGill University, Montreal, QC, Canada, H3A 2B4

[3]School of Automation, Northwestern Polytechnical University; Xian, 710000, China.

*Corresponding author. Email: xijiang@uestc.edu.cn

Abstract: Mental processing delineates the functions of the human mind encompassing a wide range of motor, sensory, emotional, and cognitive processes, each of which is underlain by the neuroanatomical substrates. Identifying accurate representation of neuroanatomical substrates of mental processing could inform understanding of its neural mechanism. The challenge is that it is unclear whether a specific mental process possesses a 'neuroanatomy fingerprint', i.e., a unique pattern of neuroanatomy that determines the mental process. We used multi-task deep learning to disentangle the neuroanatomy fingerprint of a mental process from other multiple mental processes. The neuroanatomy fingerprint is a unique set of functional activity strength of whole-brain regions with high discrimination ability (AUC = 0.99) among different mental processes. The functional activity strength distribution of neuroanatomy fingerprint unveils both common and distinct brain regions involved in different mental processes. The neuroanatomy fingerprint also addresses a long-standing hypothesis: At least in Chinese and US populations, there consistently exists a neuroanatomy fingerprint to underlie the associated mental process.

One-Sentence Summary: Each mental process has a neuroanatomy fingerprint, which is represented as a unique pattern of functional activity strength of whole-brain regions, to differentiate from other different mental processes.

Main Text: The brain receives, encodes, stores, retrieves, and manipulates information as mental processing to delineate brain functions. More than two centuries ago, it was proposed that the human-specific mental processing could be determined based on the shape of the skull (*1*). Although the theory of phrenology was discredited in scientific research, the hypothesis that different brain regions are associated with distinct functions has been supported in a series of studies conducted thereafter (*2-6*). Consequentially, the brain atlases were established to understand the relationship between brain anatomy and function (*7, 8*). However, it is not possible to accomplish a specific process solely by relying on individual regions. These areas separated regionally on the brain atlases, may be linked together in a functional way to achieve a specific functionality(*9-14*). Different brain regions form networks corresponding to specific functions (*15*), while the same region may be involved in multiple networks to achieve different functions (*16-19*).

The high complexity of the brain often leads us to only consider a few specific brain regions and their intrinsic connections when studying a particular mental process (*20, 21*). Traditional methods such as region-wise activation t-tests can only identify active regions specific to the current process and exists a priori knowledge (*22*), while methods like dictionary learning (*23*), ICA (*24*), and PCA (*25*) may select only a few important features without fully utilizing them and fail to identify this set of fingerprints accurately. Different mental processes may activate different brain regions. An obvious question arises as to whether those areas that are not 'activated' under a given mental process are really unimportant, and how much are they actually involved in that mission? Therefore, we want to systematically analyze this problem on a whole-brain scale.

Drawing inspiration from the concept of inter-individual brain region connectivity fingerprints(*26*), we hypothesize that not only connectivity characteristics but also activation patterns of brain regions can serve as representations of the brain neuroanatomy fingerprint. At the group level of mental processing, there exists a unique set of fingerprints that represent the functional activation weights of various brain regions, and these fingerprints can effectively distinguish this process from other different mental processes.

In this research, we employ a multi-task classification approach called vision transformer (ViT) (*27*) to classify different mental processes based on functional connectivity (FC) matrices derived from fMRI data. We suppose that this model can accurately identify each process's unique fingerprints by fully utilizing these features and with zero priori assumptions that distinguish each process from the others. Using an interpretable algorithm (*28*), we extract a set of weight values from the trained model in whether a regional or connectional perspective. Our findings reveal the unique fingerprints of each mental process. Occipital lobe is the most important lobe for distinguishing among different processes, with common regions between processes primarily concentrated in the occipital and parietal lobes, while distinct regions are widely distributed across various lobes. Additionally, connections associated with the sulci are more important than those associated with the gyri. Finally, our results show consistency between different brain atlas and two populations, Chinese and US.

Result

Characteristics of subject and model inputs

In our study, we utilized the Human Connectome Project S1200 young dataset (HCP-YA) as the primary analysis dataset which consists of 1007 subjects that includes data for all seven different mental processes (emotion, gambling, language, motor, relational, social, and working memory), and used the Chinese Human Connectome Project (CHCP) dataset as the validation dataset for our conclusions which consists of 229 subjects that includes the same seven processes. To ensure the model's stability, we conducted six times five-fold cross-validation with adversarial learning techniques to obtain thirty trained parameters for our model. Each model provided us the functional weight value of each region and connection using an interpretable algorithm (Fig. 1A). With high accuracy around 93% and high AUC around 0.99, we hypothesis that the model correctly recognizes these features. Here we used the Desikan-Killiany (DK) atlas (68 gyri/sulci regions + 19 subcortical regions) as the main atlas and the conclusions in each dataset were validated on the Schaefer atlas (100 gyri/sulci regions + 19 subcortical regions).

Overview of functional fingerprints across each mental process

Initially, we displayed the weight values of neuroanatomical regions in different mental processes under the DK atlas. The model's roc curve demonstrated its reliability for multi-classification (Fig. 1C). These weight values created a unique regional fingerprint, and we assigned them to six lobes (frontal, parietal, temporal, occipital, cingulate, and subcortical). Exploring the weight distribution of these regions, we observed consistency with previous findings, such as the high weights of temporal lobe in the language and parietal lobe in the motor (Fig. 1B). However, contrary to previous results, the occipital lobe contains the most important regions in all mental processes, while subcortical regions contribute the least. Since our goal was to differentiate important regions among processes, which may differ from distinguishing resting state and task states or focusing on important regions in a single process.

To analyze our results statistically, we performed a normalization procedure considering the ratio of actual brain areas present in each lobe divided by the total number of brain areas in each lobe as a degree and add the degrees of the six lobes to compute the percentage as importance. Focusing on the top 30 percent regions, we selected 46 regions (Fig. 1D). A six-way ANOVA revealed significant differences among the six lobes in each process ($p<0.001$). Pairwise t-tests indicated that occipital regions had the highest contribution across all processes. When considering different thresholds (top 10 percent regions to top 50 percent regions with a 0.5 percent interval), occipital regions consistently exhibited the highest importance (Fig. 1E, $p<0.001$). The importance of occipital and parietal regions decreased as the importance of the other four lobes increased, except in the language where there was also a decreasing trend in the importance of the temporal lobe.

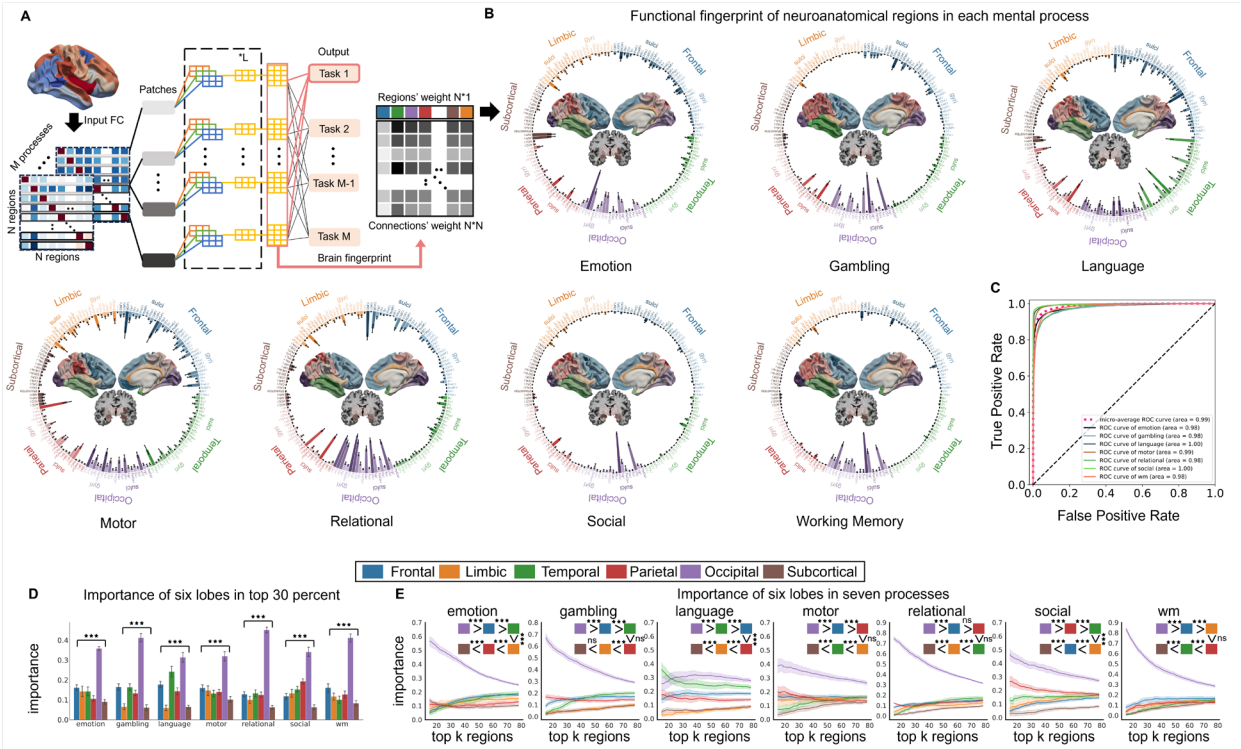

Fig.1 Neuroanatomical model reveal functional fingerprint under DK atlas. (A) To extract the neuroanatomical features from the model, we used the functional connectivity matrix as input and output both the regional and connectivity features of the model. **(B)** Functional weights of fingerprint in seven processes, we divided the brain regions into six lobes and each cortical region is divided into gyri and sulci. **(C)** ROC curves for each of the seven processes of the HCP and an average curve of the model. **(D)** Selected the most important 30 percent regions as a threshold and explore the distribution at this threshold. **(E)** Distribution of different processes from top10 (16 brain regions) to top50 (80 brain regions) under six lobes. The bar showed the mean value with confidence intervals at 95, *** and ns mean $p<0.001$ and not significant in multi-way ANOVA respectively.

Commonality and specificity in each mental process's fingerprint

We categorized the top 30 percent regions into process-common (present in all seven processes) and process-distinct (not present in all seven processes) areas and represented them in red and blue, respectively (Fig. 2A). Process-common regions were mainly located in the occipital and parietal lobes, with a few regions in the left frontal lobe. Process-distinct regions were widely distributed across all six lobes, with only a few process-common areas in the temporal and limbic lobes. The common regions in limbic lobe were mainly involved in the area close to the occipital lobe, and there were no process-common regions in the subcortical regions. However, both the left and right amygdala were involved in almost all processes.

In recent studies, since the topology of the brain surface is highly folded as gyri and sulci, several hypotheses have been proposed regarding the formation, including external factors like the limits imposed by the brain skull (*29, 30*), internal factors such as differential laminar growth (*31*), genetic regulation (*32*), axonal tension or pulling (*33, 34*). While the exact mechanism behind cortical folding remains unknown, researchers have discovered significant differences between gyri and sulci in terms of anatomy (*35, 36*), morphology (*37*), functional connectivity (*16, 38, 39*), and structural connectivity (*40*). This supports the notion that the cortical brain can be divided into two separate units: gyri, sulci.

Then we further divided the cortical regions into four categories based on the importance of gyri and sulci. Using different colored boxes, we categorized them as gyri/sulci both important, gyri/sulci both unimportant, gyri more important than sulci, and sulci more important than gyri (Fig. 2A). Within the occipital lobe, the lateral occipital (LO) region, gyri and sulci were observed to be involved in all seven processes. LO is responsible for visual stimuli formation, progressing from local to global perception (*41, 42*) which means it combines the functions of primary vision formation (concrete) to higher vision formation (abstract) (*43*). However, in other regions of the occipital lobe, such as the pericalcarine, fusiform, and lingual regions, sulci were found to be involved in all processes, while gyri participated in only a subset. These regions specialize in higher-order visual processing, such as face recognition in the fusiform region (*44-46*). In parietal lobe, there is no gyri and sulci belonging to the same brain region participating in all seven processes at the same time. The sulci of the superior parietal region are involved in all seven processes, whereas the gyri of this region active exclusively during language, relational, and social processes. The inferior parietal region's sulci were active in all processes except motor processes, while the gyri were only involved in language and social processes. These regions possess specific functions, with the superior parietal region primarily responsible for motor-sensory integration (*47*) and the orbital frontal region primarily associated with motion processing (*48*). The distribution of the temporal lobe is similar, except for language processes. The superior temporal gyri and temporal pole primarily participate in language-related processes, whereas the inferior temporal region primarily facilitates the remaining six processes. An intriguing difference is found in the frontal lobe, particularly in the medial orbitofrontal region in left hemisphere. Here, the sulci are consistently active across all seven processes, while the gyri of these regions do not exhibit involvement in relational and social processes. We also observed widespread activation in the inferior frontal region across most of the processes. In limbic, these activated areas are mostly the areas that gyri are more important than sulci, which is contrast to other four cortical lobes, where sulci are more important, or gyri/sulci are both important. These results highlight the different importance and roles of gyri and sulci in performing processes. The areas where they appear together are mainly concentrated in the visual area, while sulci are more involved in areas responsible for higher functions or specific functions, indicating the specificity of sulci under different processes.

Next, we focused on the statistical distribution of gyri and sulci in cortical areas (Fig. 2B, C). Employing a five-way ANOVA, we detected significant differences among these five groups ($p<0.001$). After pairwise t-tests, we revealed that gyri primarily influenced occipital regions in unique regions, except for the language. In contrast, only relational and working memory processes contributed the most to occipital regions in sulci. Moreover, our results indicated that sulci were more involved in higher-order areas, such as the frontal and

limbic regions than gyri. For common regions, occipital regions continued to display the highest contribution in both gyri and sulci.

To further examine these regions, we divided them into three groups: gyri, sulci, and subcortical regions. Since the number of gyri and sulci regions differs from the number of subcortical regions, we normalized the original numbers as we did to six lobes. Three-way ANOVA was conducted, depicting significant differences among the seven groups ($p<0.001$). Subsequently, pairwise t-tests were performed between each pair of subgroups. We found sulci play a more prominent role in all seven processes while subcortical regions contribute the least, gyri in the middle (Fig.2D). Then we chose top 10 to top 50 percent regions with a 0.5 percent interval finding consistent results compared with top 30 percent (Fig. 2E, $p<0.001$). The importance of the gyri/sulci/subcortical at each threshold is plotted on a line graph, revealing there are decreasing trend in gyri and sulci while an increasing trend in subcortical regions. The result is completely different from previous results that indicate gyri are a more significant hub in brain (*38, 40*). This may be due to previous studies focusing on exploring the differences between the resting state and task states, or solely investigating the properties of gyri and sulci in the brain under the resting state. However, our finding is consistent with evidence suggesting that sulci are associated with higher-frequency brain functions (*39*) and perform specific processes (*49, 50*). Notably, amygdala emerged as an important subcortical region across most processes except relational, as it is responsible for emotion, motivation, memory, and is a key component of the limbic system (*51-54*). The information flow from outside the brain is relayed through neurons to the amygdala, which subsequently communicates with the cortex (*52, 55, 56*). While subcortical regions are involved in various processes, the model primarily identified the amygdala as significant. This could be attributed to the challenge of distinguishing the specific functional differences among these subcortical regions solely based on functional connectivity patterns.

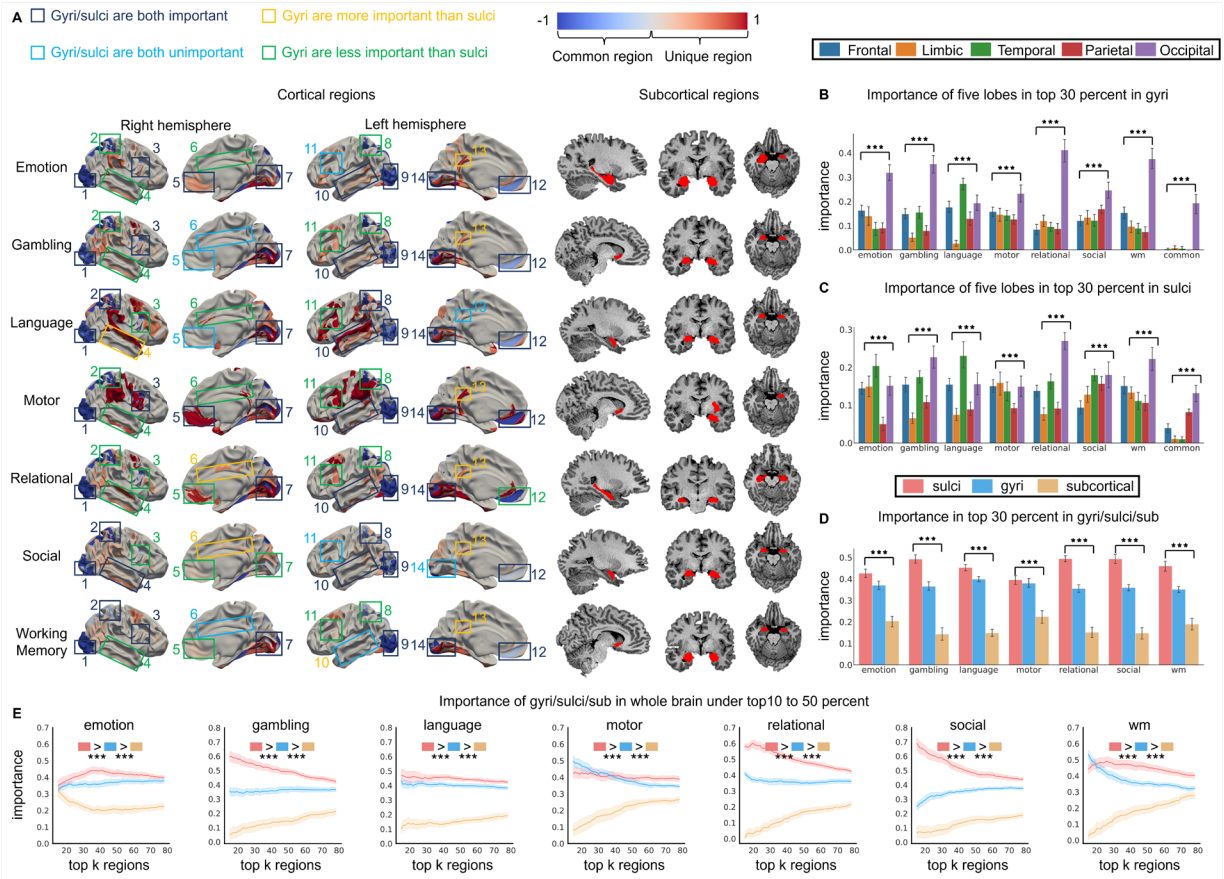

Fig. 2. Neuroanatomical features under the division of the gyri and sulci. (A) Distribution of significant fingerprints under the seven processes. We choose top 30% regions to visualize. It is an average result of 30 trained models in white matter surface and subcortical regions. Blue areas represent common regions among seven processes, read areas represent unique regions for

seven processes. At the same time, we use four different colored boxes to indicate the different properties of gyri and sulci. **(B)** Importance of gyri in five lobes in common regions and unique regions. **(C)** Importance of sulci in five lobes in common regions and unique regions. **(D)** Importance of gyri/sulci/subcortical. **(E)** Importance of different processes from top10 (16 brain regions) to top50 (80 brain regions) under gyri/sulci/subcortical. The bar shows the mean value with confidence intervals at 95, *** and ns mean $p<0.001$ and not significant in multi-way ANOVA respectively.

Validation results on CHCP and another atlas

We validated our conclusions on a completely different dataset, CHCP. By retraining the parameters of model on the CHCP dataset, the roc curve of the model showed the excellent classification ability of our model (Fig. 3A). We found that the distribution of the fingerprint of these regions across seven processes have consistent with our conclusion in HCP (Fig. 3B), and after calculating the spearman correlation coefficients of the fingerprints under these two datasets, we found a high degree of consistency under all seven mental processes (Fig. S10). For a model trained on one dataset, we found that the model can predict the other dataset with high accuracy with zero parameter updating (Fig. 3C). The model trained on HCP testing CHCP had a higher accuracy compared to model trained on CHCP testing HCP, which may be due to the difference in the number of subjects between the two datasets, as HCP has more subjects. We supposed that achieving an accuracy of around 80 with no training at all shows that the features learned by the model are generalizable. We also chose brain regions with a threshold of top30 for further analysis, we found that all seven mental processes, except motor and language, exhibit occipital is the most important lobe (Fig. 3D, $p<0.001$), and the result was consistent in any threshold (Fig. S18, $p<0.001$). Temporal contributes most in language and limbic contributes most in motor, this may be due to the different linguistic environments of the two datasets.

We then from gyri/sulci/subcortical perspective to further explore these regions. Sulci contribute most among seven processes while subcortical contribute the least, gyri in the middle (Fig. 3E). The result is consistent in any threshold (Fig. S14, $p<0.001$).

In the supplementary material, we also tested the stability of these results using another atlas, Schaefer atlas. Although using different atlases will result in inconsistent division of brain regions, different numbers of brain regions under different atlases can be divided into the same six lobes or eleven lobes (gyri and sulci division), and we compute the average weight value under each lobe dividing brain regions into six or eleven lobes. We found a high Spearman's correlation coefficient between the mean weights under the two atlases (Fig. S9). Eleven lobes showed better correlation and significance compared to six lobes, indicating that the specificity of the brain under different processes can be better demonstrated after dividing into gyri and sulci. Dividing these brain regions into six lobes showed consistency with DK atlas and from the perspective of gyri and sulci, sulci was more important than gyri in all seven processes. We also tested the stability of fingerprints under different multi-task classifications, and the results showed that the fingerprint in each process not impressed by how many processes there are, and that the fingerprints are stable for each process (Fig. S12).

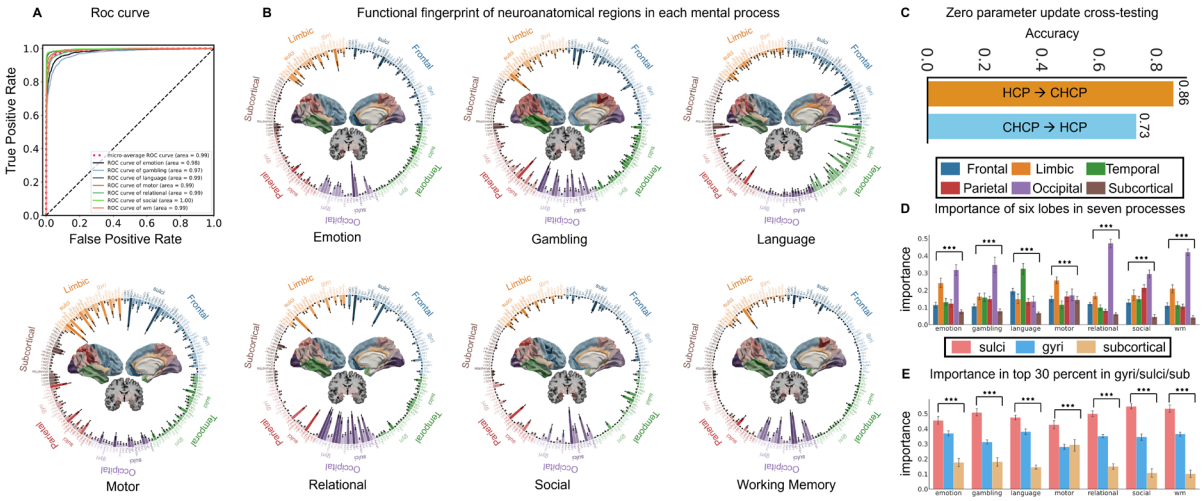

Fig. 3. Validation results on CHCP in DK atlas. (A) ROC curves for each of the seven mental processes of the HCP and the average of the curves of the model. **(B)** Importance of fingerprint regions in seven processes, we divide the brain blocks into six lobes and each cortical region is divided into gyri and sulci. **(C)** Zero parameter update cross testing. Use the model trained on HCP and CHCP respectively to explore the accuracy on the other dataset. Here we use two different brain atlases. **(D)** Importance of six lobes in seven processes in top 30 percent regions. **(E)** Importance of gyri/sulci/subcortical in seven processes in top 30 percent regions. The bar shows the mean value with confidence intervals at 95, *** and ns mean $p<0.001$ and not significant in multi-way ANOVA respectively.

Discussion

Our conclusion reveals that using the multi-task classification ViT model can effectively decode the unique fingerprint within each mental process, which is a set of values representing the functional weight of each brain region. This set of fingerprints exhibits consistency across different datasets, and their average weights under specific lobes also exhibit consistency across different brain atlases. Meanwhile, the trained model can accurately distinguish seven processes from another dataset without any parameter updates, indicating that the human brain does indeed have a set of fingerprints under a specific process, and this set of fingerprints has been verified in different populations.

Identifying specific fingerprints of the brain under each mental process helps us gain a deeper understanding of the neuroanatomical mechanisms of the brain. This recognition of the functional weight values of each brain region at the whole brain scale enables us to better understand the separation and integration of brain functions. We found that the optical lobe is the most important lobe in distinguishing different processes, and it is also the lobe with the most common regions among the seven mental processes. In addition, we also analyze the functional mechanisms of the brain from another unique perspective, gyri and sulci. The conclusion indicates that sulci play a more important role in distinguishing different processes than gyri.

Although we only used the functional connectivity matrix here, our model can also be applied to datasets in other modalities or different processes. Significantly, we only used seven mental processes from HCP and CHCP, with the two datasets mainly focusing on young people in the United States and China, aged between 22 and 35. Although these seven processes have already reflected most brain regions' activity, we can still identify more brain fingerprints under other processes. Meanwhile, due to the age limitations of our data set, it is still worth exploring whether the brain fingerprint patterns of young and elderly individuals are the same at different ages.

Materials and Methods

Participants

Two separate datasets were utilized in this study: Human Connectome Project (HCP) (*57-60*) and Chinese Human Connectome Project (CHCP) (*61, 62*).

The HCP dataset included 1,206 subjects originally, after selecting subjects who had data for all seven task states (*20*), a total of 1,007 subjects aged between 22 and 35 years (mean ± SD age of 28.72 ± 3.69 years) were included. All subjects were scanned using a customized Siemens 3T "Connectome Skyra" with a standard 32-channel Siemens receive head coil at Washington University in St. Louis. For the structural MRI T1w and T2w scans, the following parameters were used: T1w repetition time = 24,000 ms, echo time = 2.14 ms, inversion time = 1,000 ms, flip angle = 8 degrees, field of view 224 × 224 mm, voxel size 0.7 mm isotropic, bandwidth 210 Hz/Px, ipat 2, acquisition time 7:40 (minutes:seconds). T2w repetition time = 3,200 ms, echo time = 565 ms, field of view 224 × 224 mm, voxel size 0.7 mm isotropic, bandwidth 744 Hz/Px, ipat 2, acquisition time 8:24 (minutes:seconds). The functional MRI data had the following acquisition parameters: repetition time = 720 ms, echo time = 33.1 ms, flip angle = 52 degrees, field of view 208 × 180 mm, matrix 104 × 94, slice thickness 2.0 mm, 72 slices, 2.0 mm isotropic voxels, multiband factor 8, echo spacing 0.58 ms, bandwidth 2290 Hz/Px. The seven tasks (working memory, gambling, motor, language, social, relational, and emotion) had different run durations and number of frames: 5:01 minutes and 405 frames, 3:12 minutes and 253 frames, 3:34 minutes and 284 frames, 3:57 minutes and 316 frames, 3:27 minutes and 274 frames, 2:56 minutes and 232 frames, and 2:16 minutes and 176 frames, respectively.

The CHCP dataset included 366 subjects, and after selecting subjects who had data for all seven task states, 228 subjects aged between 18 and 31 years (mean ± SD age of 22.28 ± 2.84 years) were included in the analysis. All subjects were scanned using a Siemens 3T Prisma scanner in Beijing. For the structural MRI T1w and T2w scans, the following parameters were used: T1w repetition time = 24,000 ms, echo time = 2.22 ms, inversion time = 1,000 ms, flip angle = 8 degrees, field of view 256 × 240 mm, voxel size 0.8 mm isotropic, bandwidth 220 Hz/Px, acquisition time 6:36 (minutes:seconds). T2w repetition time = 3,200 ms, echo time = 563 ms, field of view 256 × 240 mm, voxel size 0.8 mm isotropic, bandwidth 744 Hz/Px, acquisition time 6:22 (minutes:seconds). The functional MRI data had the following acquisition parameters: repetition time = 710 ms, echo time = 33.0 ms, flip angle = 52 degrees, field of view 212 × 212 mm, matrix 104 × 94, slice thickness 2.0 mm, 72 slices, 2.0 mm isotropic voxels, multiband factor 8, echo spacing 0.57 ms, bandwidth 2358 Hz/Px. The number of frames varied for each of the seven tasks: 411 frames for resting, 253 frames for working memory, 288 frames for gambling, 321 frames for motor, 278 frames for language, 236 frames for social, 202 frames for relational, and 202 frames for emotion.

Data preprocessing

To extract signals from the datasets, we utilized ICA-FIX MSMAll grayordinate data (41). The HCP dataset had already done minimal preprocessing and can be directly downloaded from the HCP website at https://www.human-connectome.org/. However, as the CHCP dataset did not provide minimal preprocessing datasets, we employed the HCP pipeline (v4.7) to process the CHCP dataset, which can be found at https://github.com/Washington-University/HCPpipelines. This allowed us to process the CHCP dataset in a consistent method with the HCP dataset, forming the basis for further analysis. The minimally preprocessing procedure involved the following steps: prefreesurfer, freesurfer, postfreesurfer, fmrivolume, fmrisurface, ica-fix, and msmall, more detailed information can be found in this paper (*63*).

Functional connectivity

First, we extracted the brain signals from the grayordinate data, which consists of 96,854 vertex and pixel measurements. Specifically, 64,984 vertexes were corresponding to cortical regions and 31,870 pixels were corresponding to subcortical regions. To further analyze these grayordinate data, we employed different brain atlases to test the stability of our results. Our primary analysis was based on the widely used Desikan-Killiany (DK) atlas, which contains 68 cortical regions (*7*). Additionally, we validated our findings using the Schaefer atlas, which contains 100 cortical regions (*8*). For subcortical regions, we used the automatic parcellation atlas

provided by Freesurfer which consist of 19 regions. We then divided the cortical brain regions into gyral/sulcal areas based on the sulc value (*64*). For cortical regions, positive sulc values represented gyri, while negative values represented sulci. Gyri correspond to the convex parts of the brain surface, while sulci represent the concave parts. The cortical regions' gyral/sulcal division was determined using a threshold set after the HCP minimal processing pipeline. Based on the previous study, the selected top or bottom value had no influence on the consistency of the final result (*65*). Here, we selected the top and bottom 20% of sulc values in each region to consider them as gyri or sulci. Unfortunately, subcortical regions cannot be divided into gyral/sulcal units due to technical shortcomings. By applying the thresholds, we successfully determined whether a region corresponds to a gyral or sulcal area.

In DK atlas, there exits 155 regions and in Schaefer atlas there exits 219 regions. To compute the functional similarity between brain regions, we calculated the average signal within each region. Subsequently, we employed the widely used Pearson correlation to quantify the functional connectivity between the signals of pairs of regions:

$$P_{S_{i,}S_j} = \frac{cov(S_{i,}S_j)}{\sigma_{S_i} * \sigma_{S_j}}$$

Where the $S_{i,}S_j \in S = [S_{1,}S_2, \dots S_n]$ $(n = num\ of\ cortical\ regions)$ represents individual brain region and $cov(.)$ and $\sigma_{(.)}$ represent the covariance and standard deviation respectively. For each subject, we can calculate their seven tasks functional connectivity matrix which will be used in our model.

<u>Vision Transformer model</u>

Here we use Vision Transformer (ViT) model (*27*) as the main framework of our multi-task classification model. The ViT model of the classification block is shown in Fig. S1, it contains three major parts, including embedding (patch and position), N*transformer blocks, and a fully connected layer. We will introduce these three parts in following paragraphs.

First, we convert the FC matrix to a list of sequences as the input of our model. Since the FC matrix is a single channel image, the dimensions of one FC are only two dimensions, so our input can be represented as $x \in R^{H*W}$, where the H and W are high, width of FC matrix respectively. Also, due to the nature of the FC matrix, its high and width both represent the number of brain regions we get under a specific atlas, so the values of H and W are the same here. We convert the FC matrix into patches that do not overlap with each other from $x \in R^{H*W}$ to $x_p \in R^{N*P_h*P_w}$, where N is the number of patches and P_h and P_w is the high and width of each patch. Unlike the traditional patch size such as 16*16 or 14*14 when processing natural pictures, here we use one row or one column of the FC as a patch, because we suppose such a row or column can represent the functional characteristics of one brain region. So N is equal to H and W, and $P_h = 1, P_w = W\ or\ P_w = 1, P_h = H$. Since we get N patches, for each patch, as patch contain W or H vectors, we put the patch into a trainable linear projection layer which will transfer the patch $x_p^i \in R^{P_h*P_w}, x_p^i \in x_p = [x_p^1, x_p^2 \dots x_p^N], i = 1 \dots N$ into $x_p^{i'} \in R^{1*D}$ where D denotes the target dimension. Here we set D as 784. So, the patches can be converted into $x_{pa} \in R^{N*D}$. In additional, we add an additional positional information which has the same dimension as patch embedding, $x_{po} \in R^{N*D}$. The positional embedding is added to retain positional information. Then we add an extra class token $z_{cls} \in R^{1*D}$ at the front of the patch embedding. Finally, we take the sum of patch embedding and positional embedding as input to entry the transformer block. Then the total sum of embedding is $x_{pec} \in R^{(N+1)*D}$. Third, the transformer block is consisting of two subblock, one muti-head self-attention (MSA) block and one Multi-Layer Perception (MLP) block. Each block has a layernorm ahead. Layernorm block is used to standardize the input image. It will keep the output the same dimension as input. The next layer is a muti-head self-attention. Here we use K heads to divide the input $x_{pec} \in R^{(N+1)*D}$ into $x'_{pec} \in R^{(N+1)*K*D'}$. The $D' = \frac{D}{K}$ represent the dimension for input that each self-attention layer accepts. The MSA accept q, k, v which represent query, key, value respectively form $x_{pec}^{i'} \in R^{(N+1)*D'}$, $Q = W^Q * x_{pec}^{i'}, K = W^K * x_{pec}^{i'}, V = W^V * x_{pec}^{i'}$($W^Q, W^K, W^V \in R^{d_{Q,K,V}*(N+1)}$). The attention formula is as:

$$ATTENTION(Q,K,V) = SOTMAX\left(\frac{Q * K^T}{\sqrt{d_k}}\right)V$$

Where the d_k is the same as $d_{Q,K,V}$. Then we concatenate the output of all K heads and put it into MLP layer. After N times of transformer block, we take the result of class token z_{cls} as the final output and use it to classify. Here we use 12 blocks and use a MLP to classify. We use five-fold cross-validation to give the model an average result.

Adversarial Training in ViT

By adding the calculated perturbation noise to the original image, the classifier may can correctly classify the original image and incorrectly classify the image with the perturbation even the amplitude of this perturbation is very small (*66, 67*). Human eye will not figure out these pictures, but it can easily "trick" the deep neural network during the classification stage. Hence, we add adversarial training in our model to increase the robustness of our model. In addition, some previous work indicates that gradient in the model with adversarial training is more stable and the visualization result is also more stable (*68*). Thus, adding adversarial training can benefit the interpretability of model. Here we use Fast Gradient Method (FGM) (*67*) to generate adversarial samples. The constrained perturbation can be defined as:

$$g = \nabla_x L(\theta, x, y)$$
$$r_{adv} = \epsilon g / ||g||_2$$

Where the θ is parameters of a model, x is the input of a model and y is the target associated with x. And the $L(\theta, x, y)$ is the loss of the model and ∇_x represent the derivation of x for $L(\theta, x, y)$. The basic idea of adding perturbation is following the direction of the gradient ascent, and for every step, we used the L_2 norm to constrain every step to get a unique r_{adv} for every training. We (1) calculated the forward loss of x and based on back propagation to obtain a gradient. (2) Then r_{adv} was calculated from the gradient of the embedding layer and add to the current embedding. (3) Then we got the adversarial sample $x + r_{adv}$ and calculated the forward loss of $x + r_{adv}$, and the back propagation got the gradient which will add it to the original gradient of x. (4) Then we restored the parameters of embedding dim at the original value. (5) Finally, the parameters were updated according to the gradient of (3). We set the perturbation factor as 0.001 here.

Interpretability of the Model

After classification, we wanted to explore the functional weight of patches to a specific task. The common idea was to extract the attention matrix of the model. Unlike directly extracting the last layer of the model's attention matrix, here we use an attribution propagation method based on Deep Taylor Decomposition (DTD) called Layer-wise Relevance Propagation (LRP) with a class-specific approach to get an attention map (*28*). This method will decompose the whole network through the last layer to the first layer by the contribution of every layer based on the back propagate relevance from the predicated class. We selected last layer of attention map and propagate it to the first layer by incorporating both relevancy and gradient information to finally get an attention map.

Specifically, Due to the model's input consisting of a class token and multiple patches, here our attention matrix is a $(N + 1) * (N + 1)$ matrix. The arrangement of the attention matrix follows the order of the input model's patches. Therefore, in this case, the class token is the first input of the model, while patch N is the last. We extracted the first row of the attention matrix to focus on the similarity of each patch to the class token. The magnitude of the weight value represented the degree of similarity between the patch and class token. Here, we defined it as functional weight because our input represents the functional connectivity matrix, which represented the functional characteristics of the brain. We could also obtain the similarity between two patches by extracting the bottom-right matrix of the model, and the corresponding conclusions were reflected in the supplemental materials.

Analysis of fingerprint of brain areas

We input the FC matrix into the interpretable model to obtain a functional weight for each patch (brain region), where we treated this weight as the importance of this brain region for the FC matrix. Since our model did a five-fold cross-validation and we used six different random seeds (1998-2003 here), we could get thirty parameters for the model to ensure the robustness of our result. For each parameter of the model, we put test subjects to the interpretable model, and we could get an average result from test subjects. To be more specific, for each subject as we had seven states, we put each FC matrix of one state into the interpretable model with its real label, then the model output a list of values for each patch. We treated these values as the importance of each patch to this state and the patch represents brain region. So, we got N*1 values for each subject under a specific state. For each state, we could compute the average result by sum all values from output of test subjects and then we can get an average value for each region. Since we had thirty models, we can get thirty values for each region in each state.

Then for each task, we first showed the distributional weights of the brain fingerprints under each task, and by subdividing the brain regions into six lobes (Frontal, Parietal, Temporal, Occipital, Cingulate, Subcortical), we could quantitatively identify the most important regions under different brain atlas. We then selected different thresholds to get the most important regions to explore the robustness of our results. Then we could group these regions into gyri, sulci, and subcortical regions or six lobes to do a further analysis. Due to the values of gyri, sulci, subcortical regions, or the number of six lobes are inconsistent, we need to perform a simple standardization of their values by using:

$$normolized\ number = \frac{real\ number * \max value\ of\ all\ subgroup}{value\ for\ this\ subgroup}$$

After the normalization, we use the normalized values to calculate the percentage of each component.

Analysis of fingerprint of brain connections

We input the FC matrix into the interpretable model to obtain a weight matrix, where we treat this score as the importance of the connections between two patches. Since patches are corresponding to brain regions, we get the importance of each two regions. For each parameter of the model, we compute an average result from test subjects for each state by averaging all test subjects' values. Then we can get thirty values for each connection in each state. Since we have gyri, sulci, and subcortical areas, three types of brain regions, we can have six types of connections (gyri-sulci, sulci-sulci, gyri-gyri, sulci-sub, gyri-sub, sub-sub). By choosing top values from different thresholds, we can get the different number of connections. Due to the values of gyri, sulci, subcortical regions, or the number of six lobes are inconsistent, we need to perform a simple standardization of their values by using:

$$normolized\ number = \frac{real\ number * \max value\ of\ all\ subgroup}{value\ for\ this\ subgroup}$$

After the normalization, we use the normalized values to calculate the percentage of each component. And we can map these connections into six lobes to explore where these connections locate in.

Graph theory in brain networks

For the average weight FC matrix, we can take different thresholds to get sparse matrixes, and we believe these significant connections constitute a brain network reflecting the involvement of various regions of our brain under this task. Therefore, we want to use four different graph-theoretic metrics to calculate the properties of the brain network. Here we chose degree, betweenness centrality, shortest path length, and clustering coefficient to reflect the situation of each region in the brain. The degree represents the connectivity of the node with other nodes, and a higher degree value indicates that the node is approximately important. The higher the degree, the more important the node is in the network. The shortest path length represents the average of the shortest path from this node to all other nodes, which reflects the communication ability between this node and other nodes. The clustering coefficient represents the local nature of the node and illustrates the local properties of the node. And betweenness centrality represents the number of times the node is passed in the number of shortest path entries from one node to another. We wanted to explore the global and local properties of brain regions using these four formulae.

Fig. S1

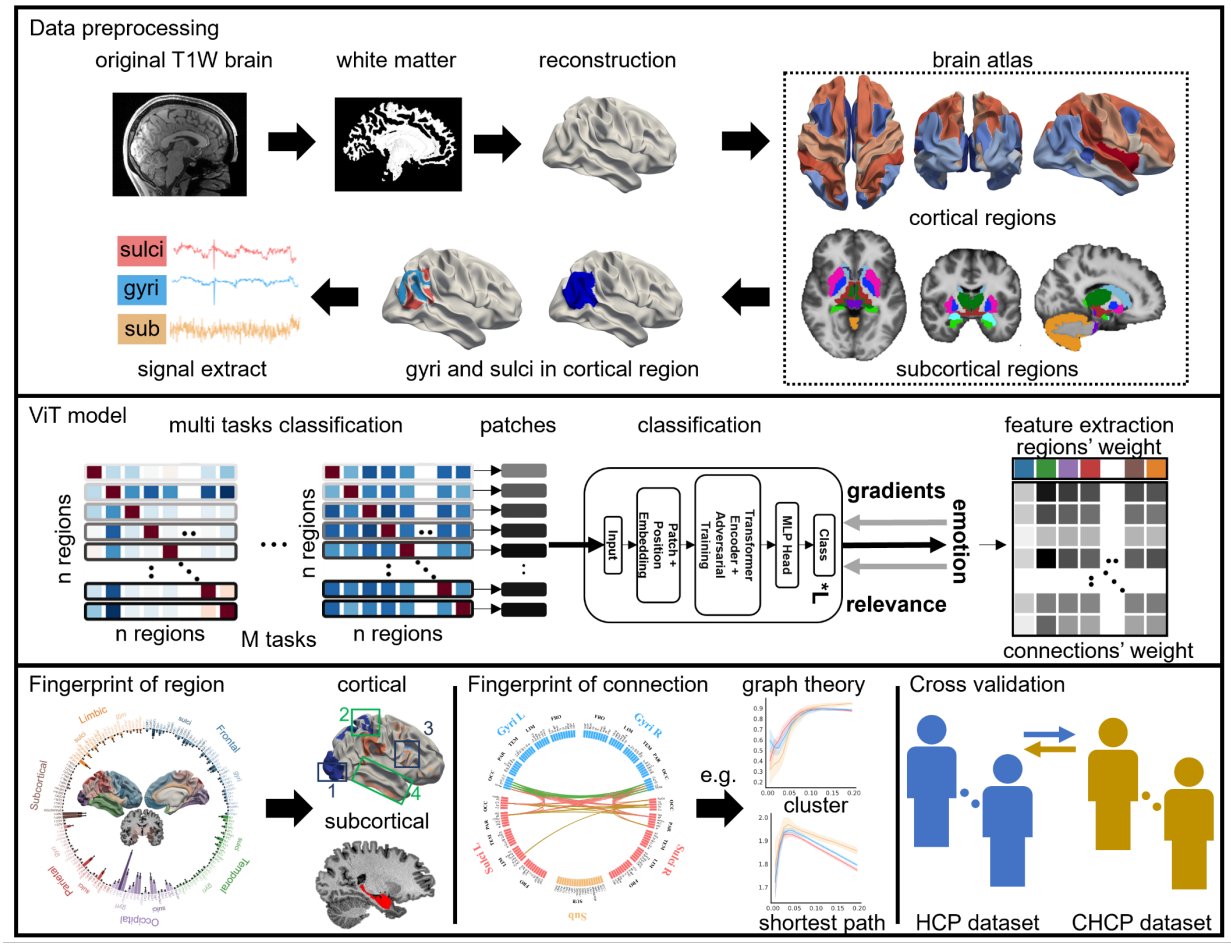

Fig. S1: *Overview of our method.* It contains three parts, data preprocessing, classification model, region, and connection analysis. *Data preprocessing*: First we preprocess CHCP data using HCP pipeline, and extract signals from the reconstructed surface of cortical region of gyri and sulci and pixel of subcortical region. *ViT model:* we use FC matrix as our input to the vit model and after training, we can use interpretable algorithm to visualize important regions and connections. *Region analysis:* we show the regional fingerprints of the brain under the task. Then explore common and unique features between tasks. *Connectional analysis:* we show the connectional fingerprints of the brain under the task. Then explore the graph theory across tasks. *Cross validation:* we use HCP dataset as our primary dataset to analysis, CHCP dataset as the validation dataset. We do training on the two datasets separately to get the conclusions and also use the trained model for cross validation.

Fig. S2

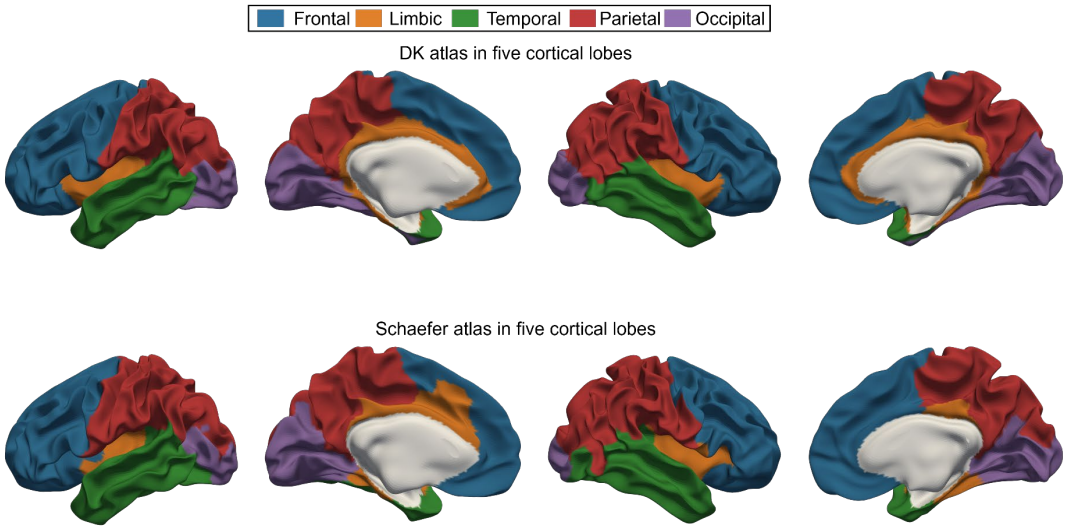

Fig. S2: *Five cortical lobes in DK and Schaefer.* In the distribution of five lobes in the cortical regions of the DK and Schaefer atlases, there is a slight difference between Schaefer and DK in the junction between some lobes due to the difference in areas delineated by the DK and Schaefer atlases, as well as the fact that we have based our baseline on the five lobes delineated by the DK atlas.

Fig. S3

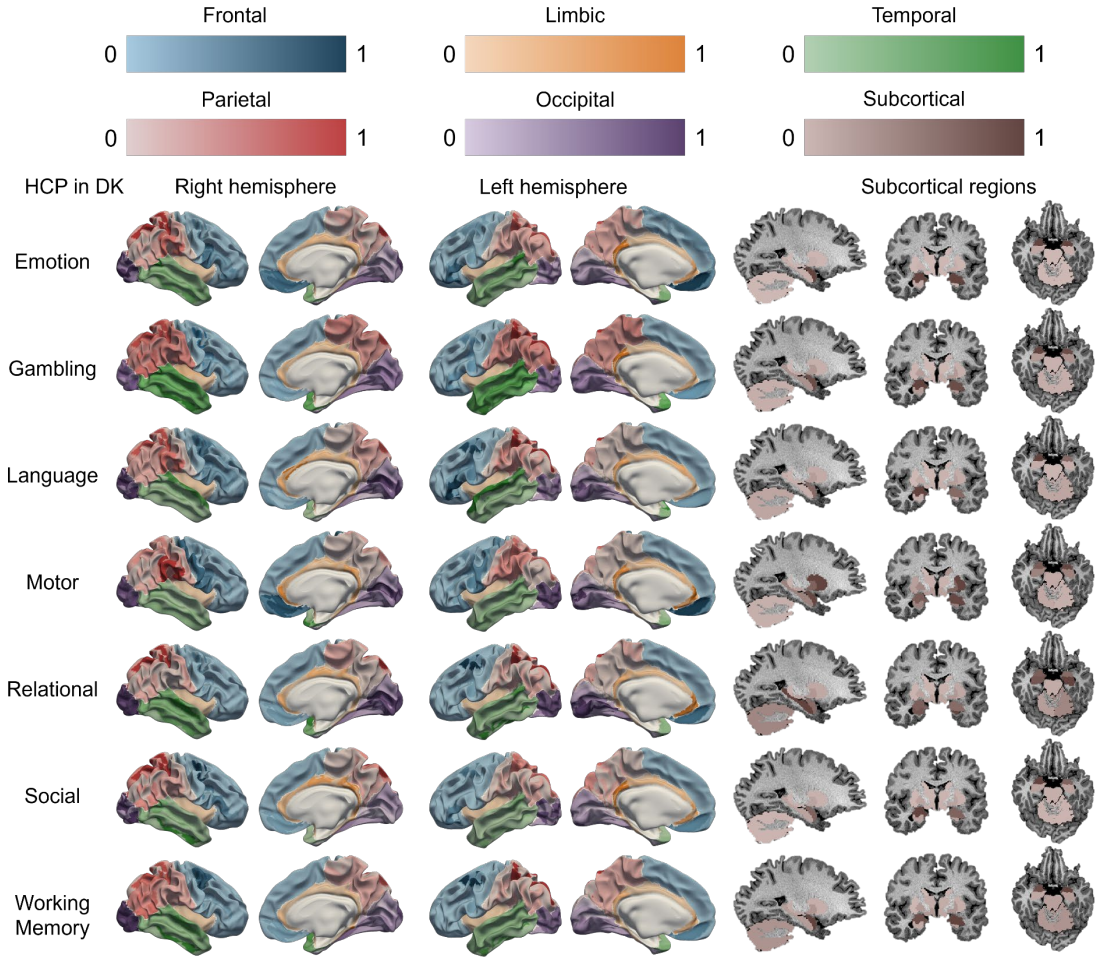

Fig. S3: Visualization of the weight values of fingerprint under six lobes in HCP in DK. Each lobe is represented as a unique color, and the weight demonstrate its importance.

Fig. S4

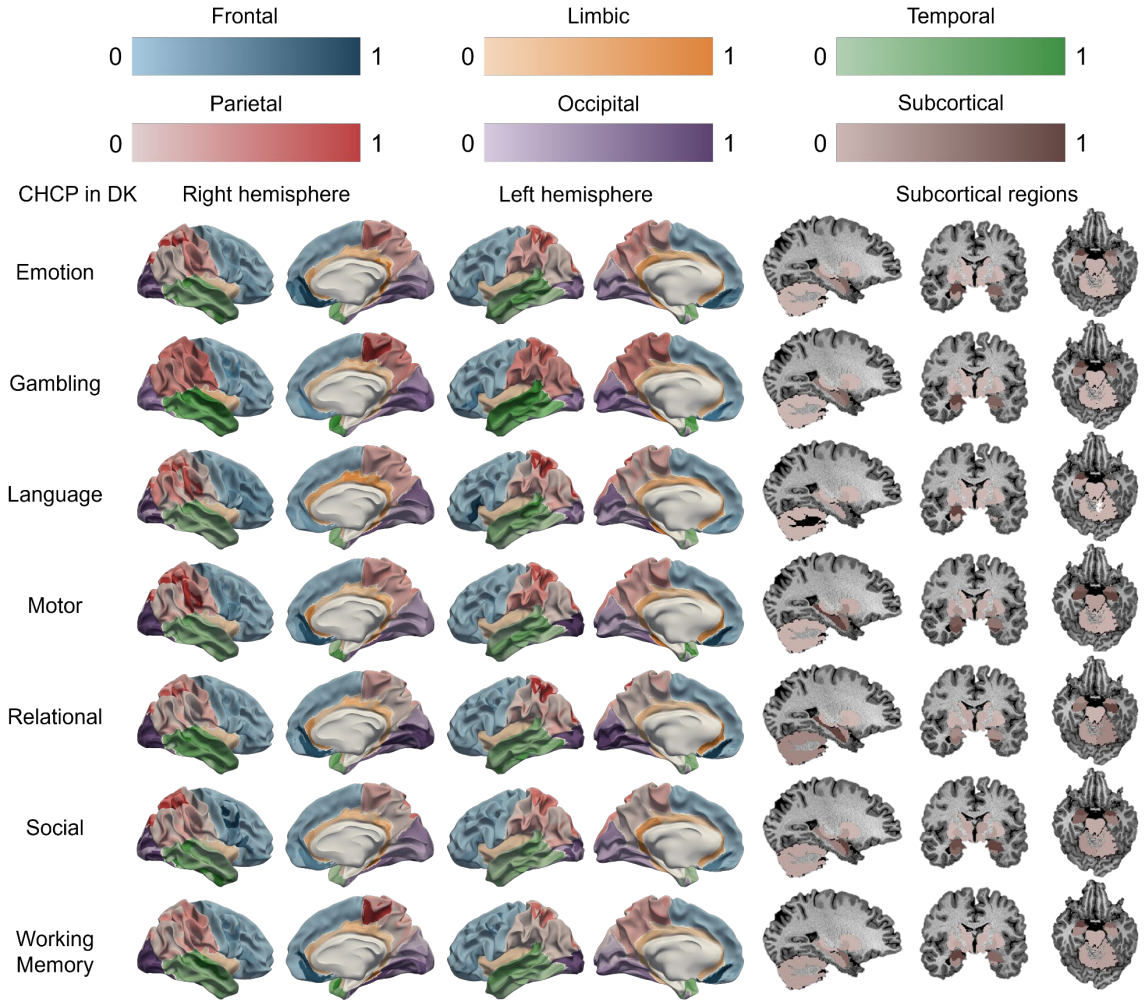

Fig. S4: Visualization of the weight values of fingerprint under six lobes in CHCP in DK. Each lobe is represented as a unique color, and the weight demonstrate its importance.

Fig. S5

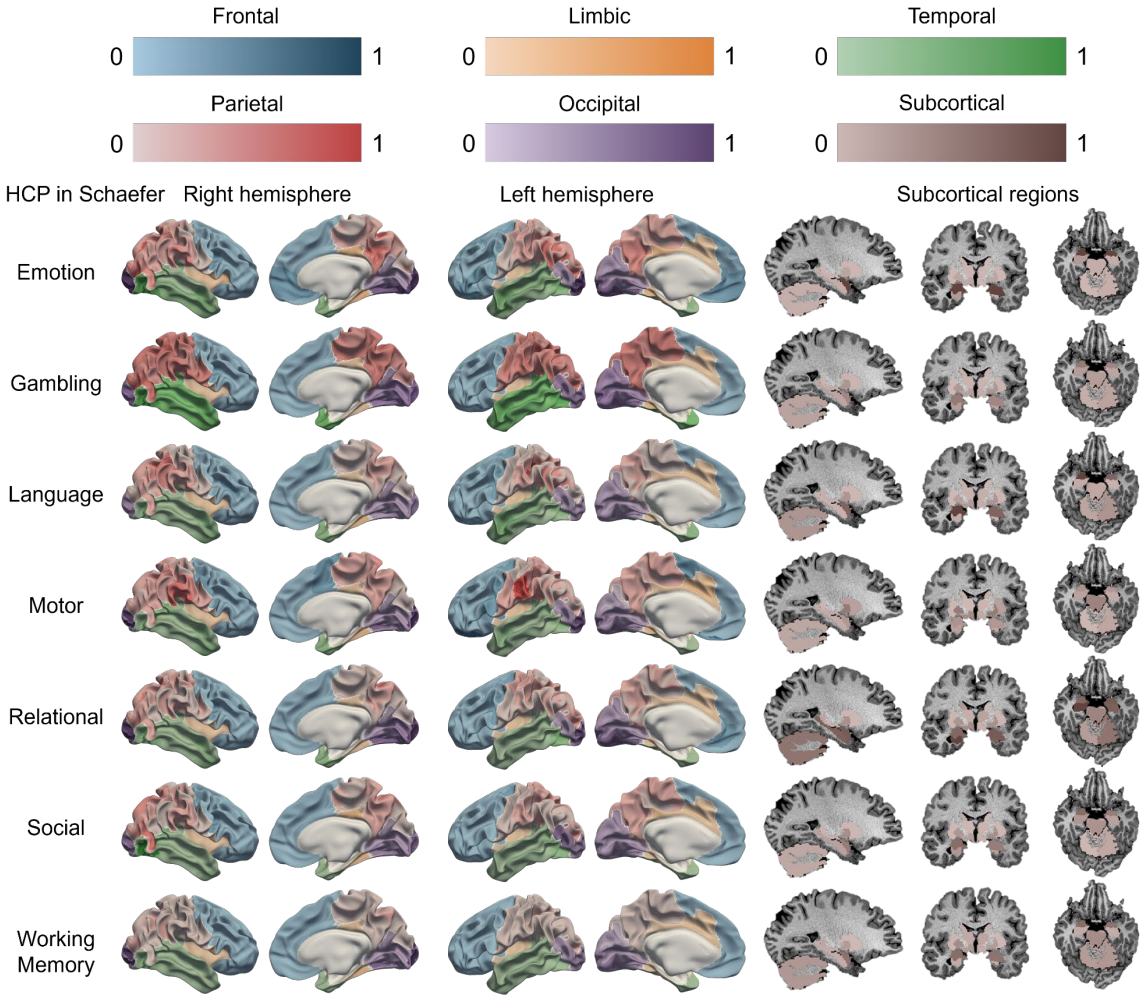

Fig. S5: Visualization of the weight values of fingerprint under six lobes in HCP in Schaefer. Each lobe is represented as a unique color, and the weight demonstrate its importance.

Fig. S6

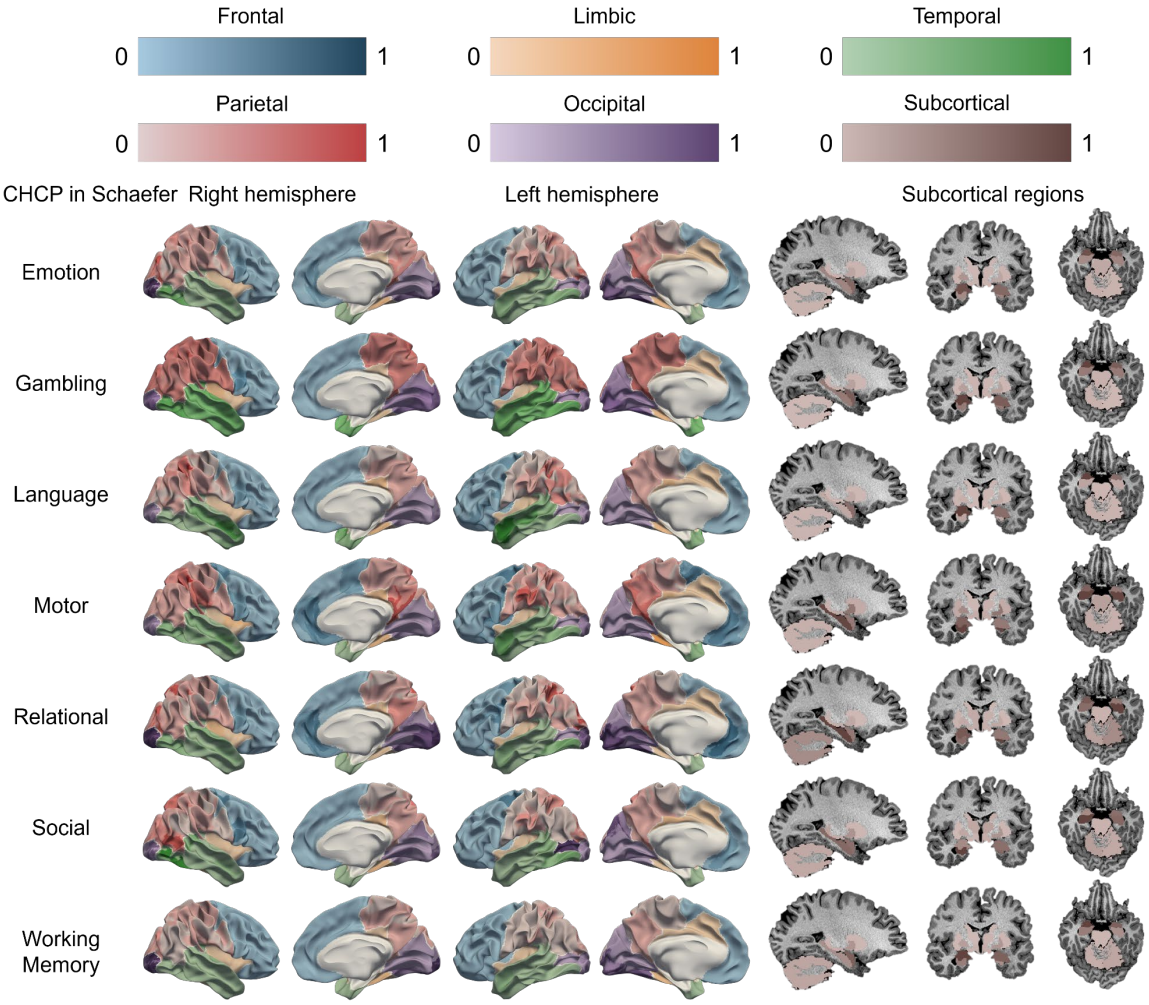

Fig. S6: Visualization of the weight values of fingerprint under six lobes in CHCP in Schaefer. Each lobe is represented as a unique color, and the weight demonstrate its importance.

Fig. S7

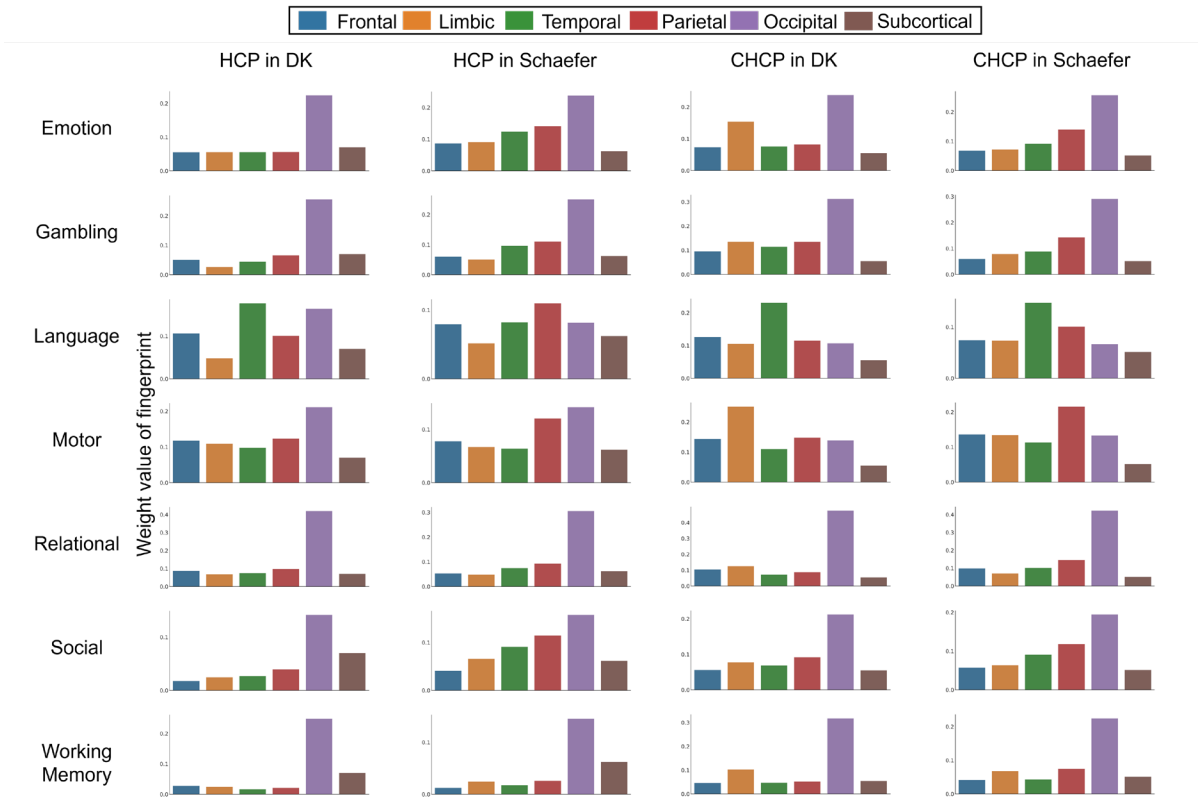

Fig. S7: Visualization of the mean weight values of fingerprint under six lobes in HCP/CHCP in DK/Schaefer atlas.

Fig. S8

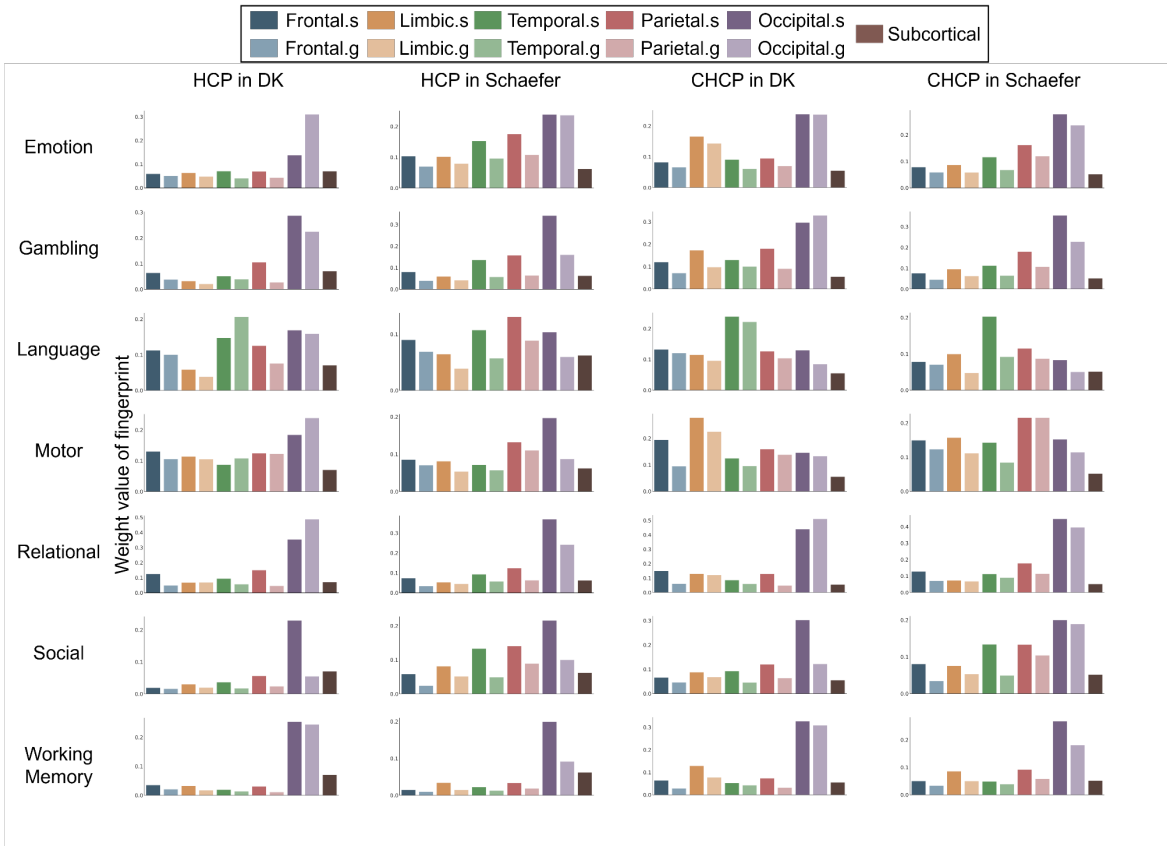

Fig. S8: Visualization the mean weight values of fingerprint under eleven lobes in HCP/CHCP in DK/Schaefer atlas, s and g represent sulci and gyri.

Fig. S9

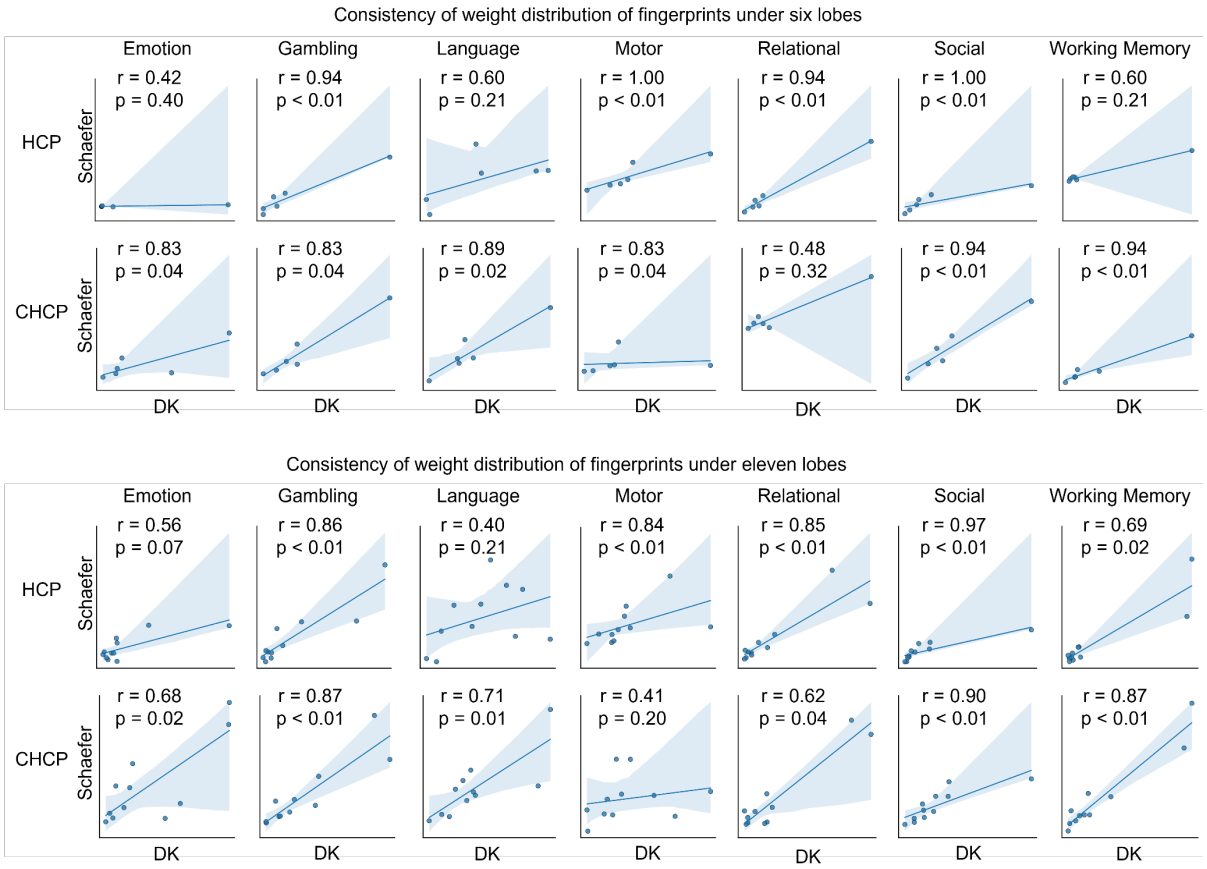

Fig. S9: Consistency of weight distribution of fingerprints under two maps. We used the DK atlas and the CHCP atlas to count the average weight values of the six lobes without gyri and sulci delineation as well as the eleven leaves after gyri and sulci delineation of the five lobes on the cortex, respectively, and to count the Spearman correlation coefficients under the two atlases.

Fig. S10

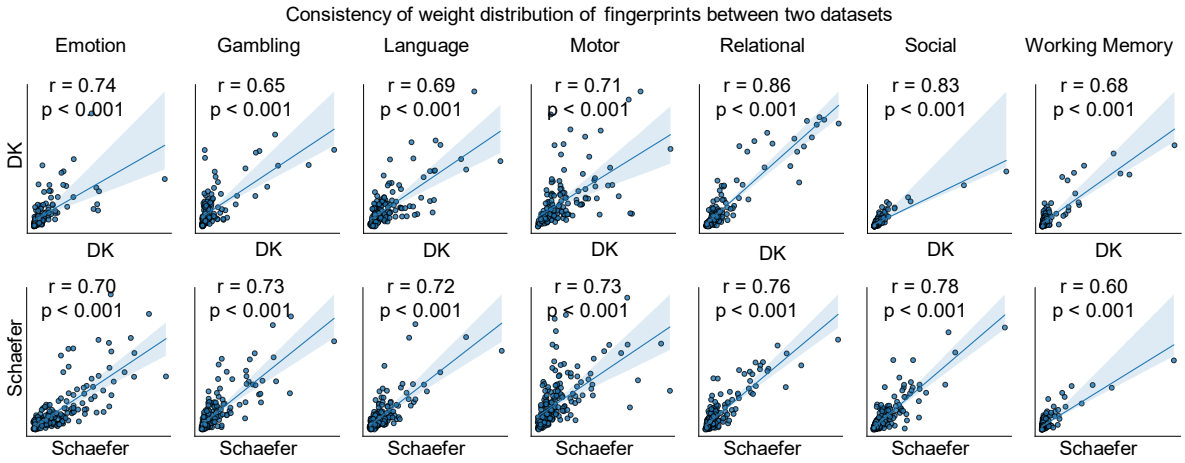

Fig. S10: Consistency of weight distribution of fingerprints under two datasets. We used DK and Schaefer atlases to explore the consistency of fingerprint in HCP and CHCP datasets. The horizontal axis of each plot is the weights under HCP and the vertical axis is the weights under CHCP, and we calculate the Spearman correlation coefficient to represent the correlation.

Fig. S11

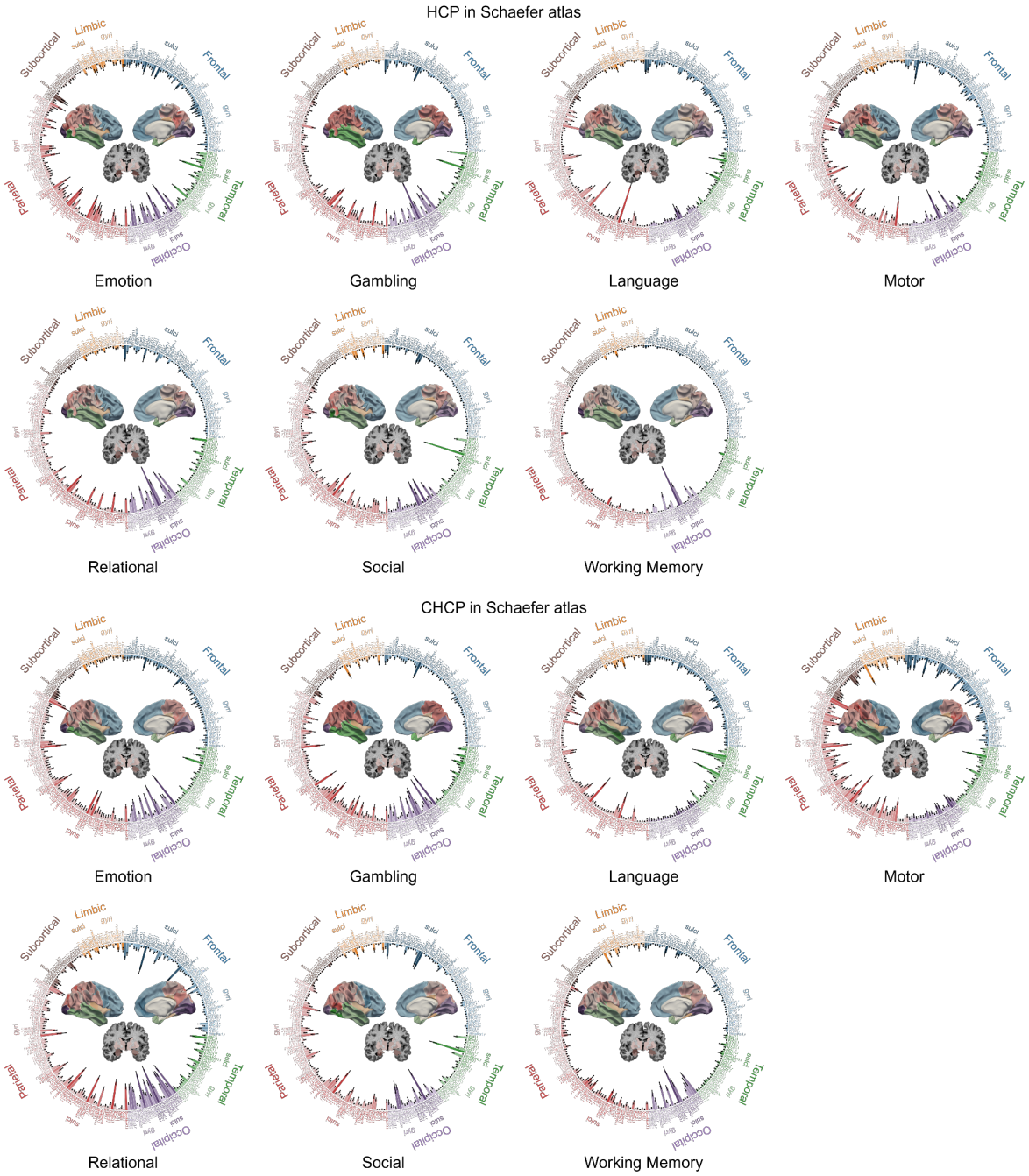

Fig. S11: Value distribution in Schaefer atlas in HCP/CHCP. Importance of each brain blocks in seven tasks, we divide the brain blocks into six lobes and each cortical region is divided into gyri and sulci.

Fig. S12

Fig. S12: Stability of fingerprints under other multi-task classification. Here, we used emotion as a benchmark and tested the stability of fingerprints under emotion from two classification to six classification, while other processes' fingerprints were also drawn.

Fig. S13

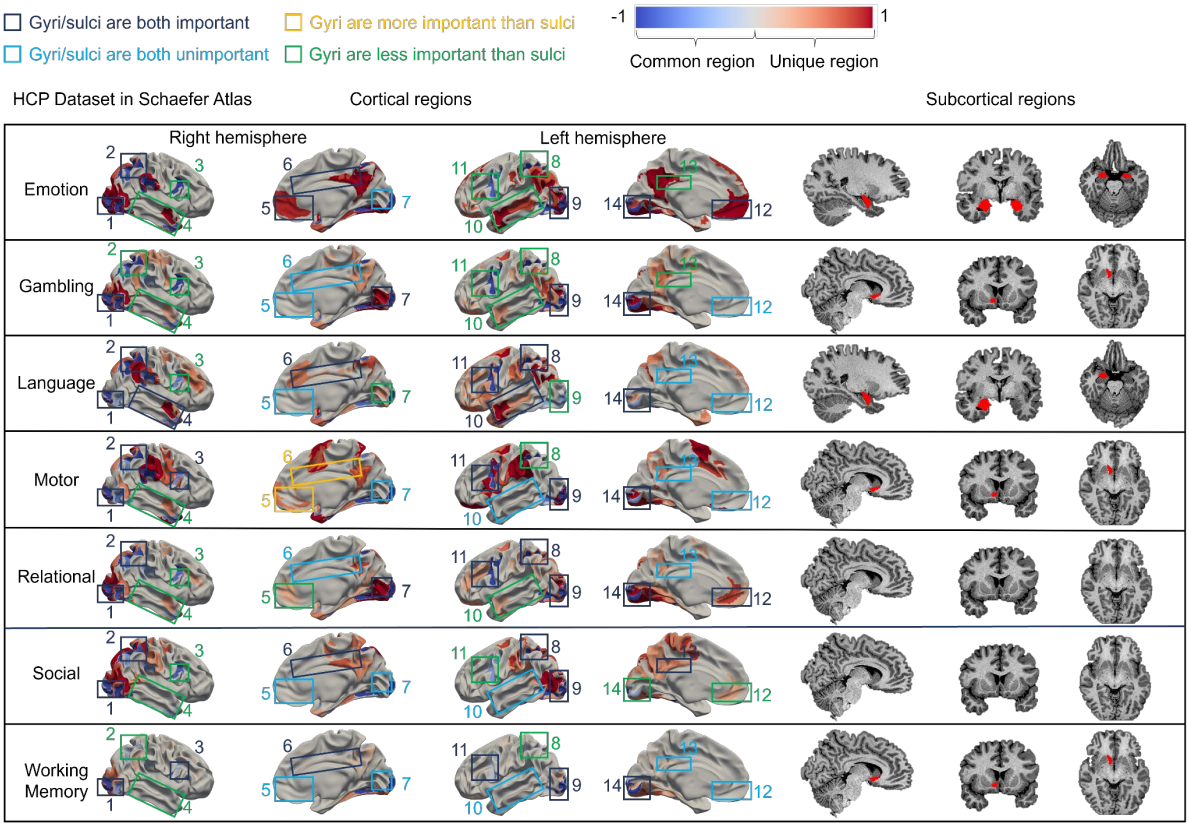

Fig. S13: Visualization on brain surface in cortical and subcortical regions in DK atlas in CHCP.

FIG. S14

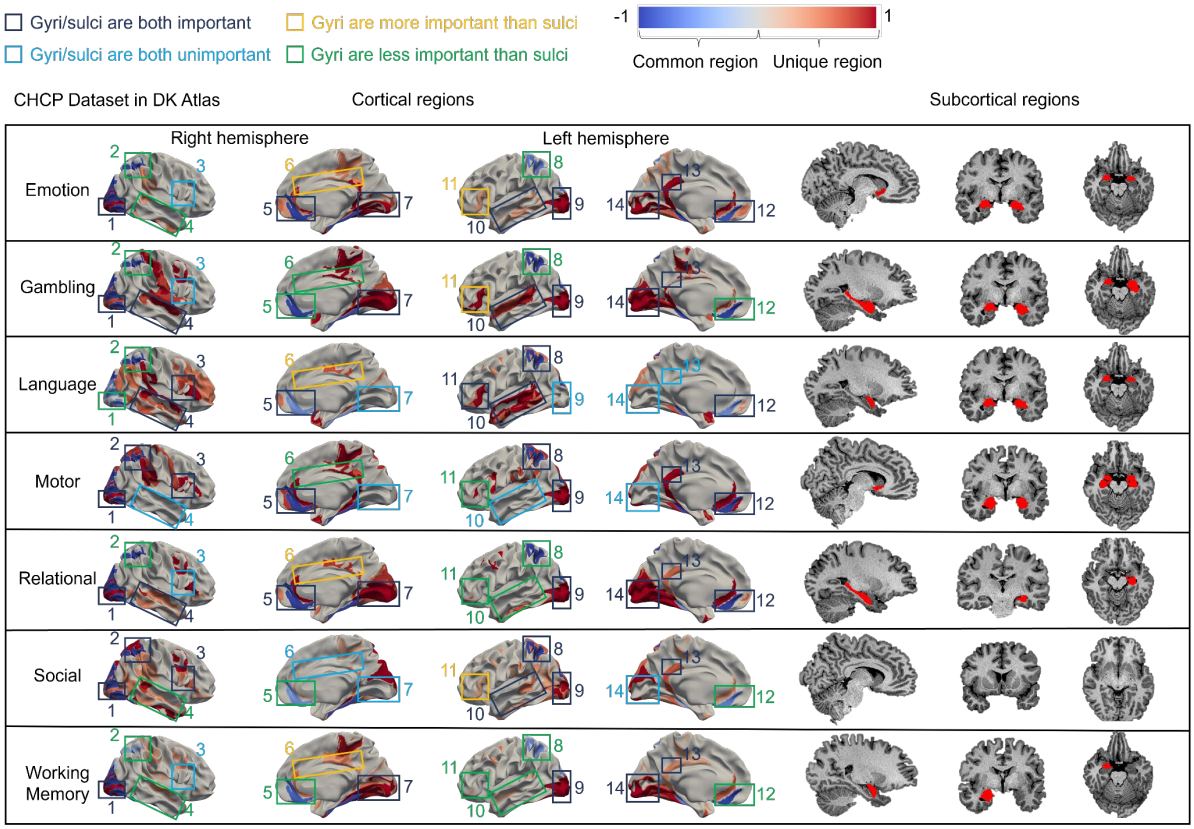

Fig. S14: Visualization on brain surface in cortical and subcortical regions in Schaefer atlas in HCP.

FIG. S15

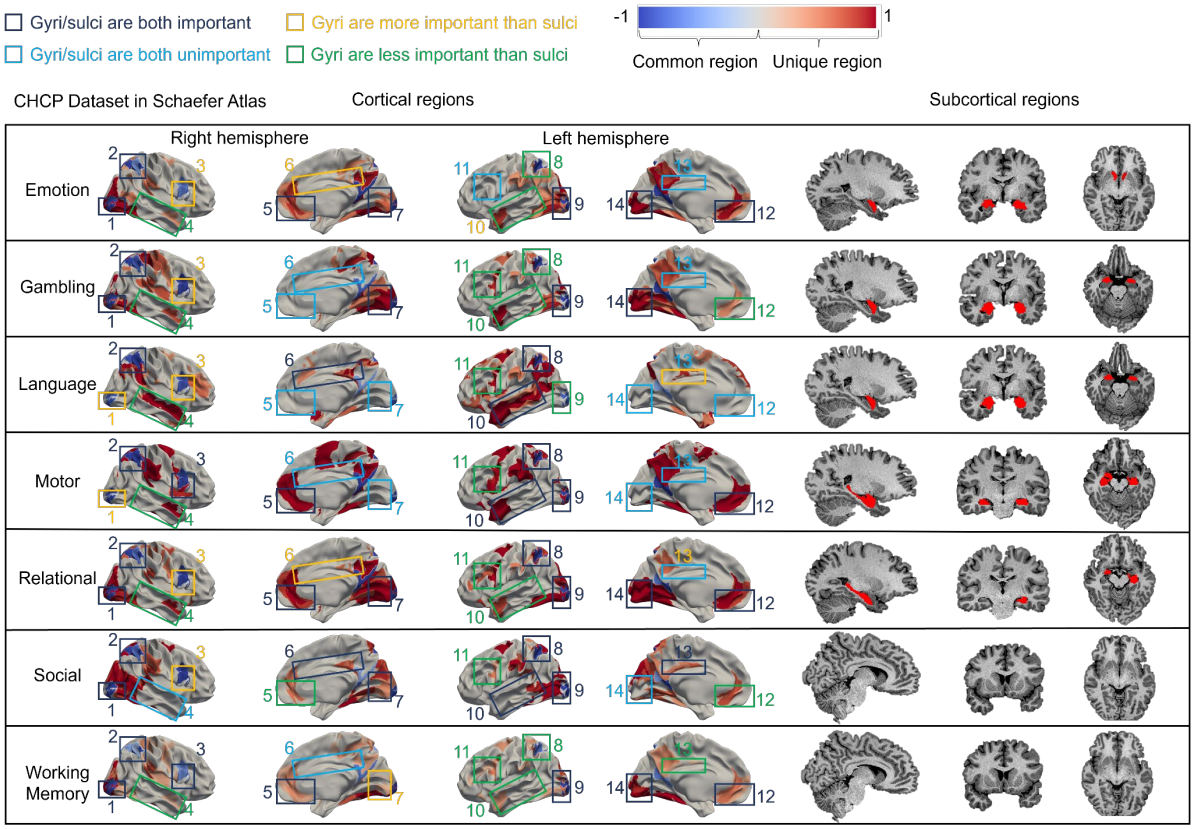

Fig. S15: Visualization on brain surface in cortical and subcortical regions in Schaefer atlas in CHCP.

FIG. S16

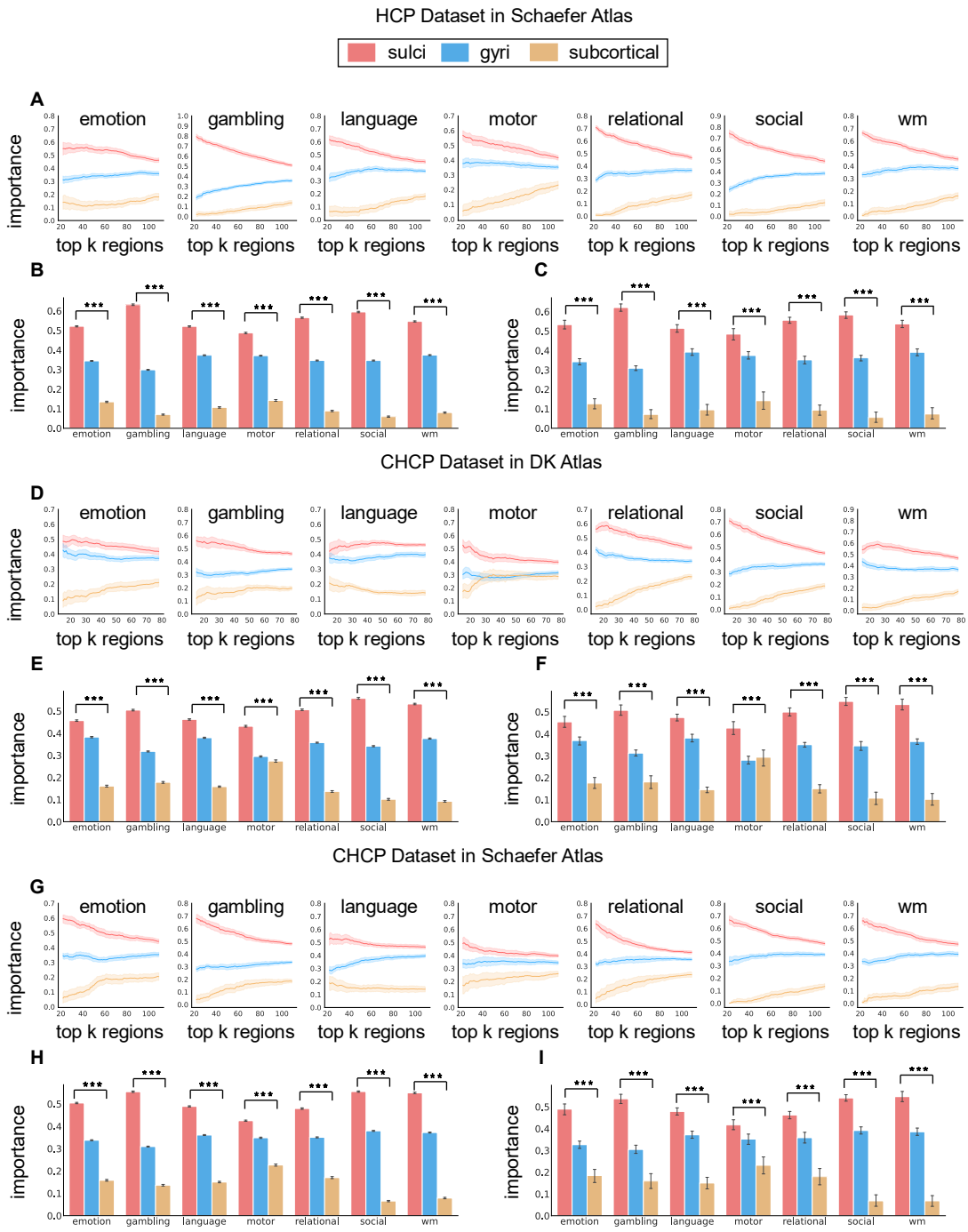

Fig. S16: Importance of gyri/sulci/subcortical regions in seven tasks **(A, D, G)** Importance of gyri/sulci/subcortical regions from top 10 percent regions to top 50 percent regions. **(B, E, H)** Statistical test for Fig. A, D, G. **(C, F, I)** Importance of gyri/sulci/subcortical in seven tasks in top 30 percent region. The bar shows the mean value with confidence intervals at 95, *** and ns mean p<0.001 and not significant in multi-way ANOVA respectively.

FIG. S17

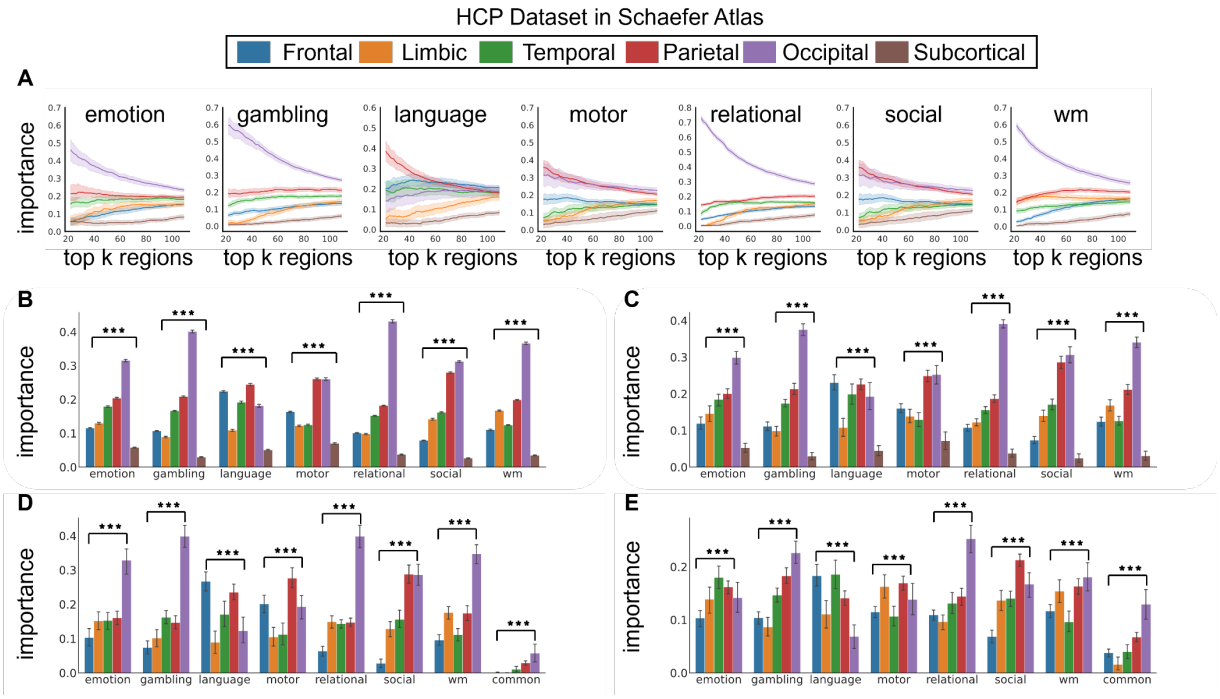

Fig. S17: Distribution of important regions in six lobes in seven tasks in HCP Schaefer atlas. **(A)** Importance of six lobes in seven tasks from top 10 percent regions to top 50 percent regions, the line with shaded area indicates the distribution of data with confidence intervals at 95. **(B)** Statistical test for Fig. A. **(C)** Importance of six lobes in seven tasks in top 30 percent regions in common regions and unique regions. **(D)** Gyri of importance of six lobes in seven tasks in top 30 percent regions in common regions and unique regions. **(E)** Sulci of importance of six lobes in seven tasks in top 30 percent regions in common regions and unique regions. The bar shows the mean value with confidence intervals at 95, *** and ns mean p<0.001 and not significant in multi-way ANOVA respectively.

Fig. S18

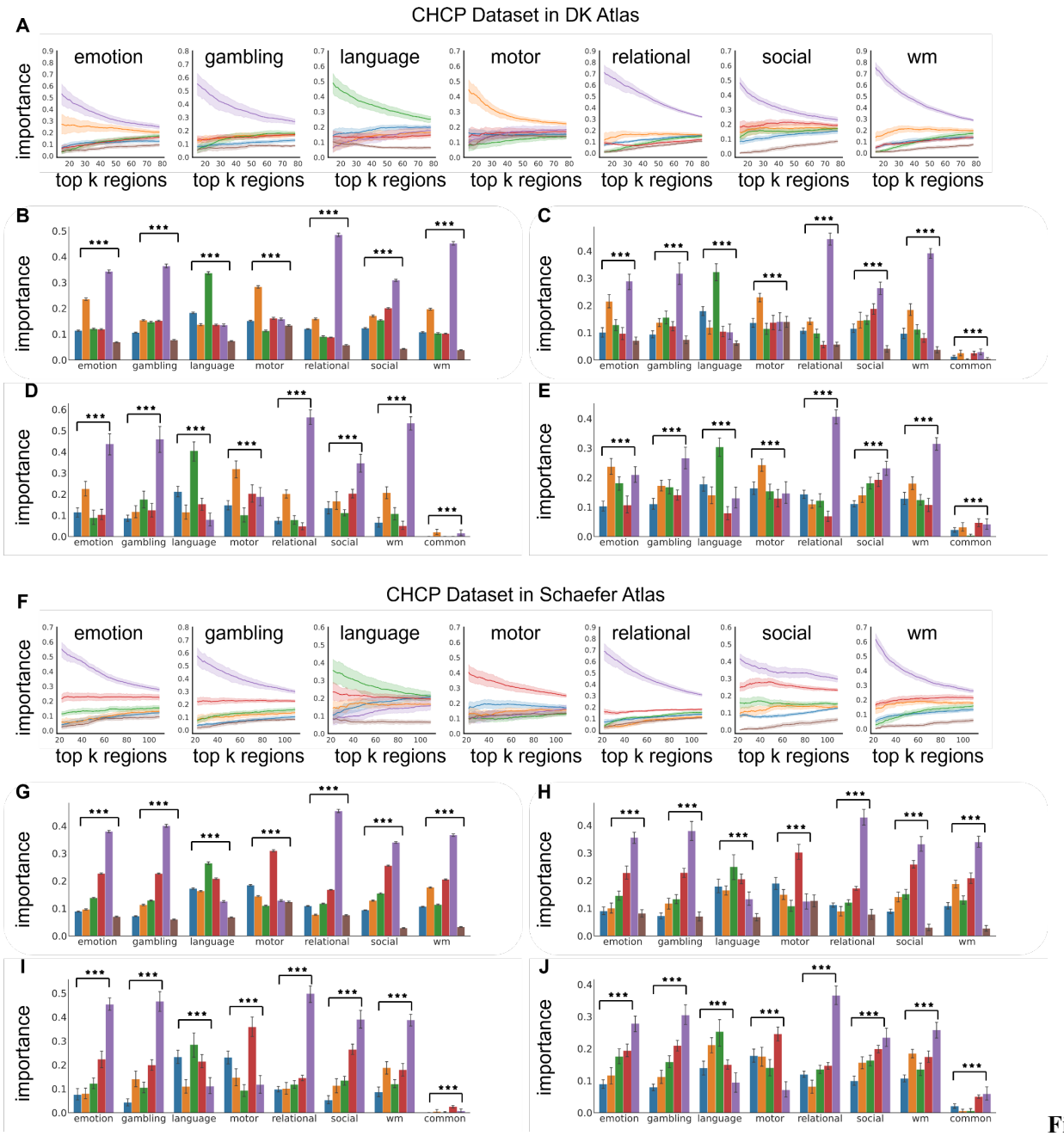

Fig. S18: Distribution of important regions in six lobes in seven tasks in CHCP in DK/Schaefer atlas. **(A, F)** Importance of six lobes in seven tasks from top 10 percent regions to top 50 percent regions, the line with shaded area indicates the distribution of data with confidence intervals at 95. **(B, G)** Statistical test for Fig. A, F. **(C, H)** Importance of six lobes in seven tasks in top 30 percent regions in common regions and unique regions. **(D, I)** Gyri of importance of six lobes in seven tasks in top 30 percent regions in common regions and unique regions. **(E, J)** Sulci of importance of six lobes in seven tasks in top 30 percent regions in common regions and unique regions. The bar shows the mean value with confidence intervals at 95, *** and ns mean $p<0.001$ and not significant in multi-way ANOVA respectively.

FIG. S19

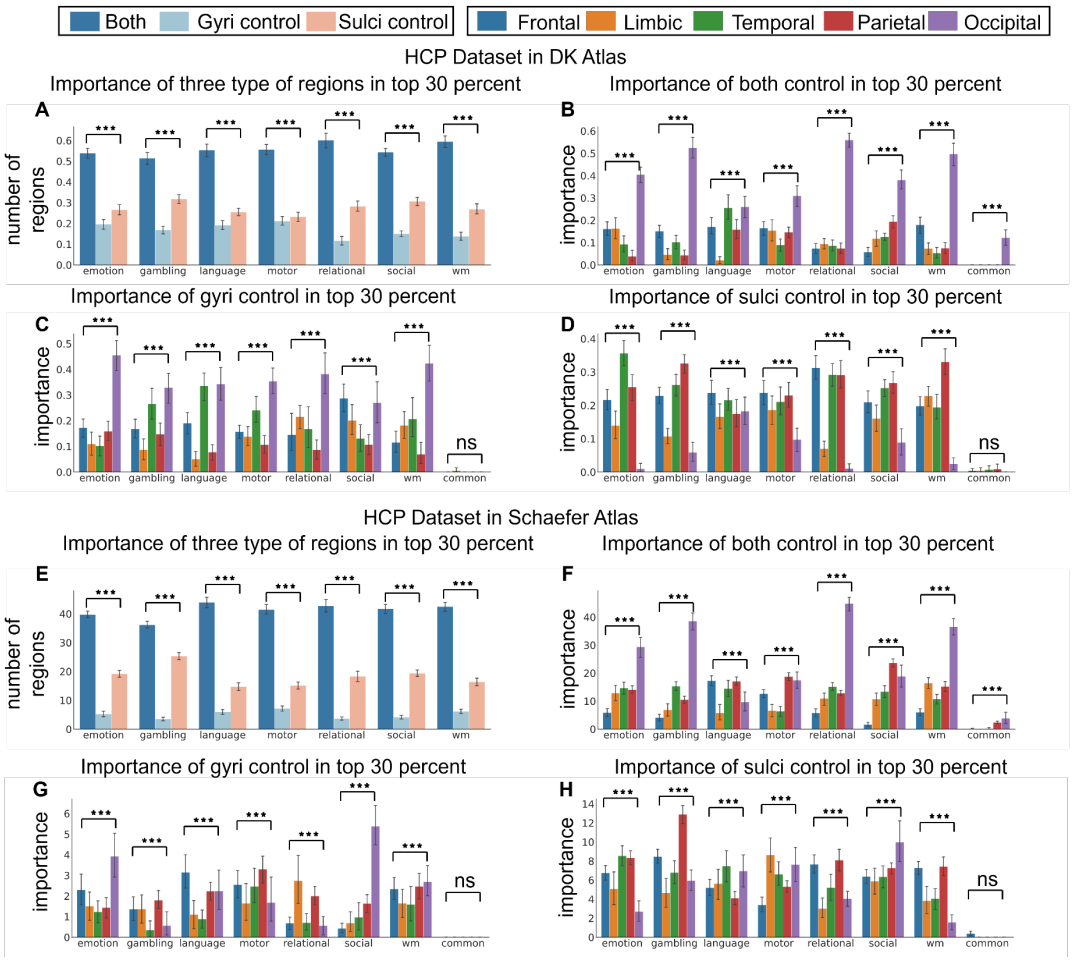

Fig. S19: Gyri/sulci-controlled regions among top 30 percent in HCP DK/Schaefer atlas. **(A, E)** number of gyri/sulci-controlled regions across seven tasks. **(B, F)** Importance of gyri&sulci-controlled regions in five cortical lobes. **(C, G)** Importance of gyri-controlled regions in five cortical lobes. **(D, H)** Importance of sulci-controlled regions in five cortical lobes. The bar shows the mean value with confidence intervals at 95, *** and ns mean p<0.001 and not significant in multi-way ANOVA respectively.

FIG. S20

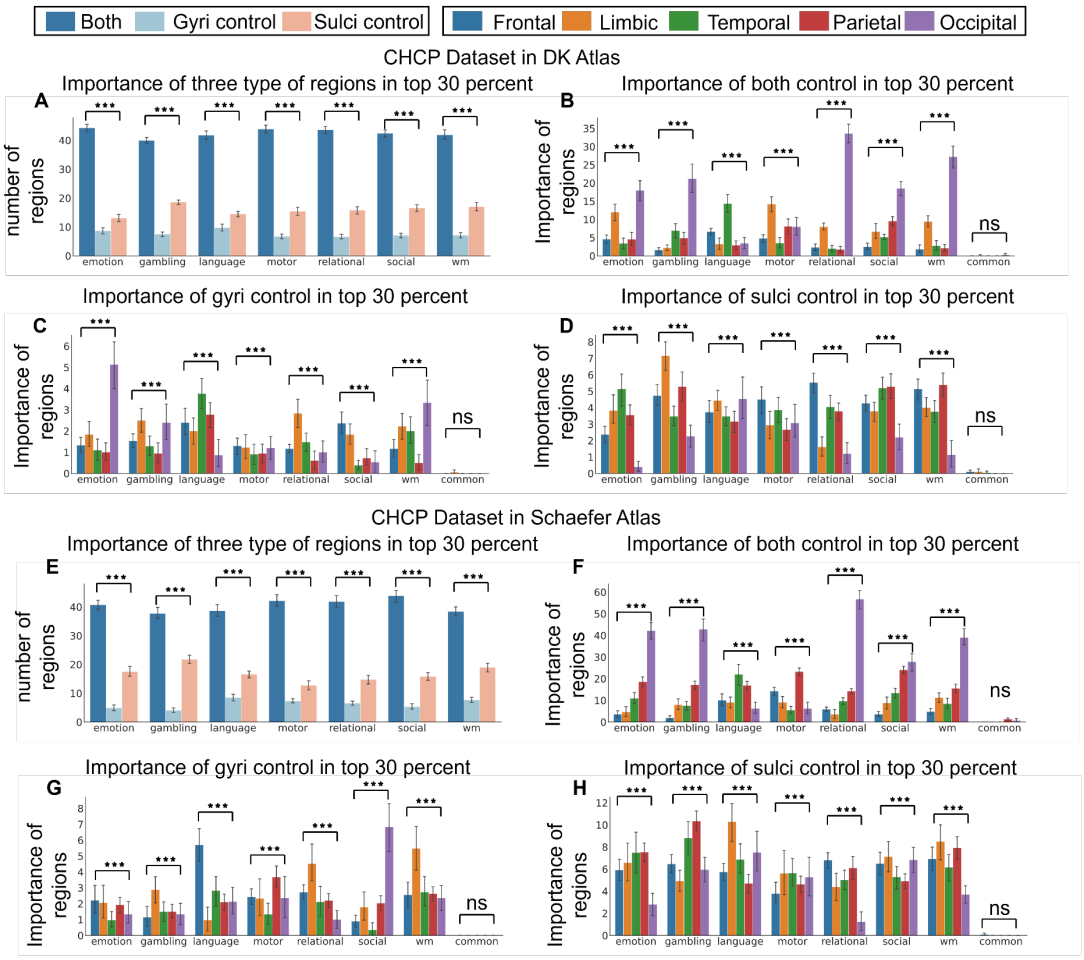

Fig. S20: Gyri/sulci-controlled regions among top 30 percent in CHCP DK/Schaefer atlas. **(A, E)** number of gyri/sulci-controlled regions across seven tasks. **(B, F)** Importance of gyri&sulci-controlled regions in five cortical lobes. **(C, G)** Importance of gyri-controlled regions in five cortical lobes. **(D, H)** Importance of sulci-controlled regions in five cortical lobes. The bar shows the mean value with confidence intervals at 95, *** and ns mean p<0.001 and not significant in multi-way ANOVA respectively.

FIG. S21

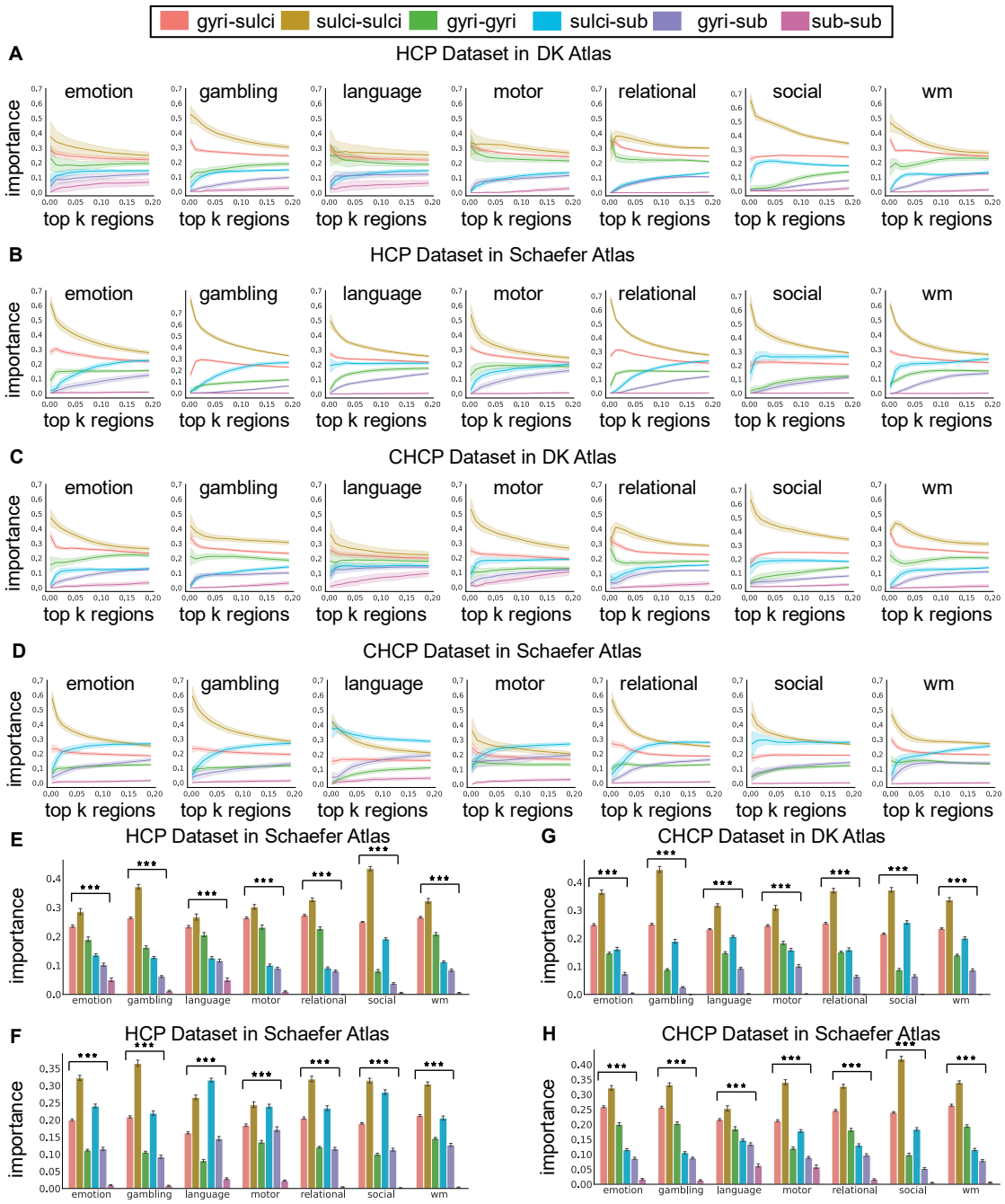

Fig. S21: Importance of six types of connections in HCP/CHCP DK/Schaefer atlas. **(A, B, C, D)** Importance of six types of connections across seven tasks. **(E, F, G, H)** Statistical test for Fig. A, B, C. The bar shows the mean value with confidence intervals at 95, *** and ns mean p<0.001 and not significant in multi-way ANOVA respectively.

FIG. S22

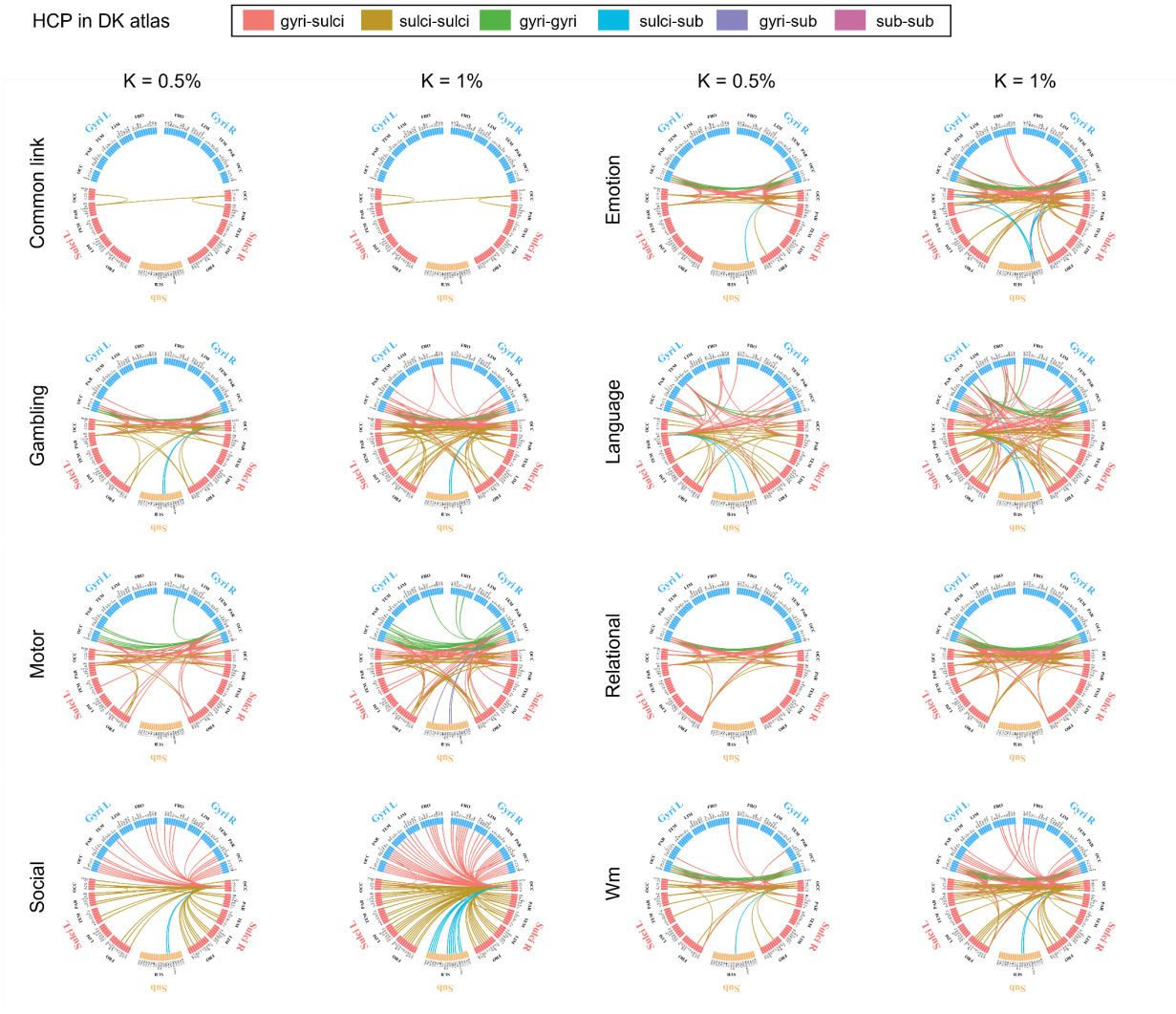

Fig. S22: Visualization of important connections in top 0.5 and 1 percent in HCP dataset in DK atlas.

FIG. S23

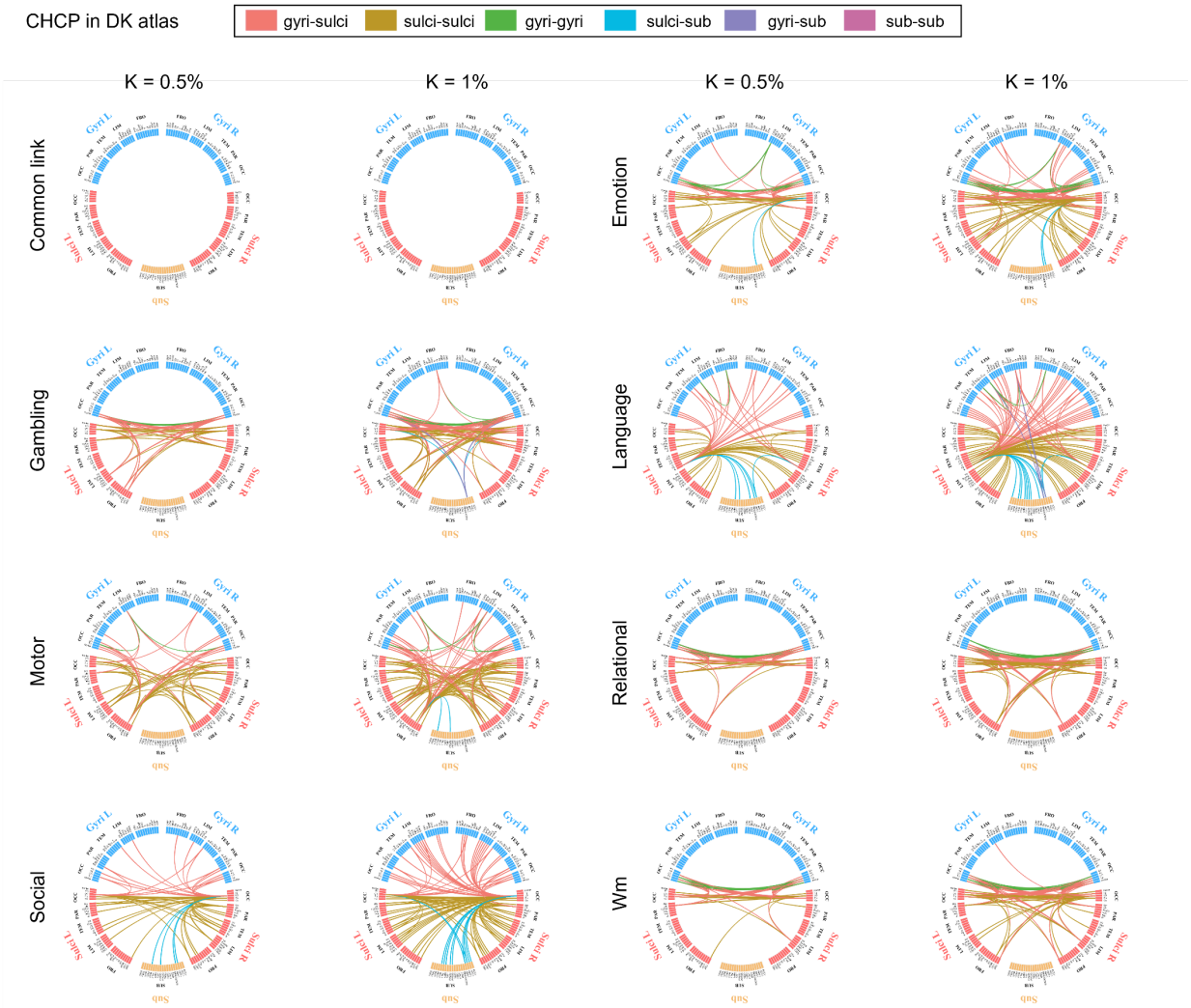

Fig. S23: Visualization of important connections in top 0.5 and 1 percent in CHCP dataset in DK atlas.

FIG. S24

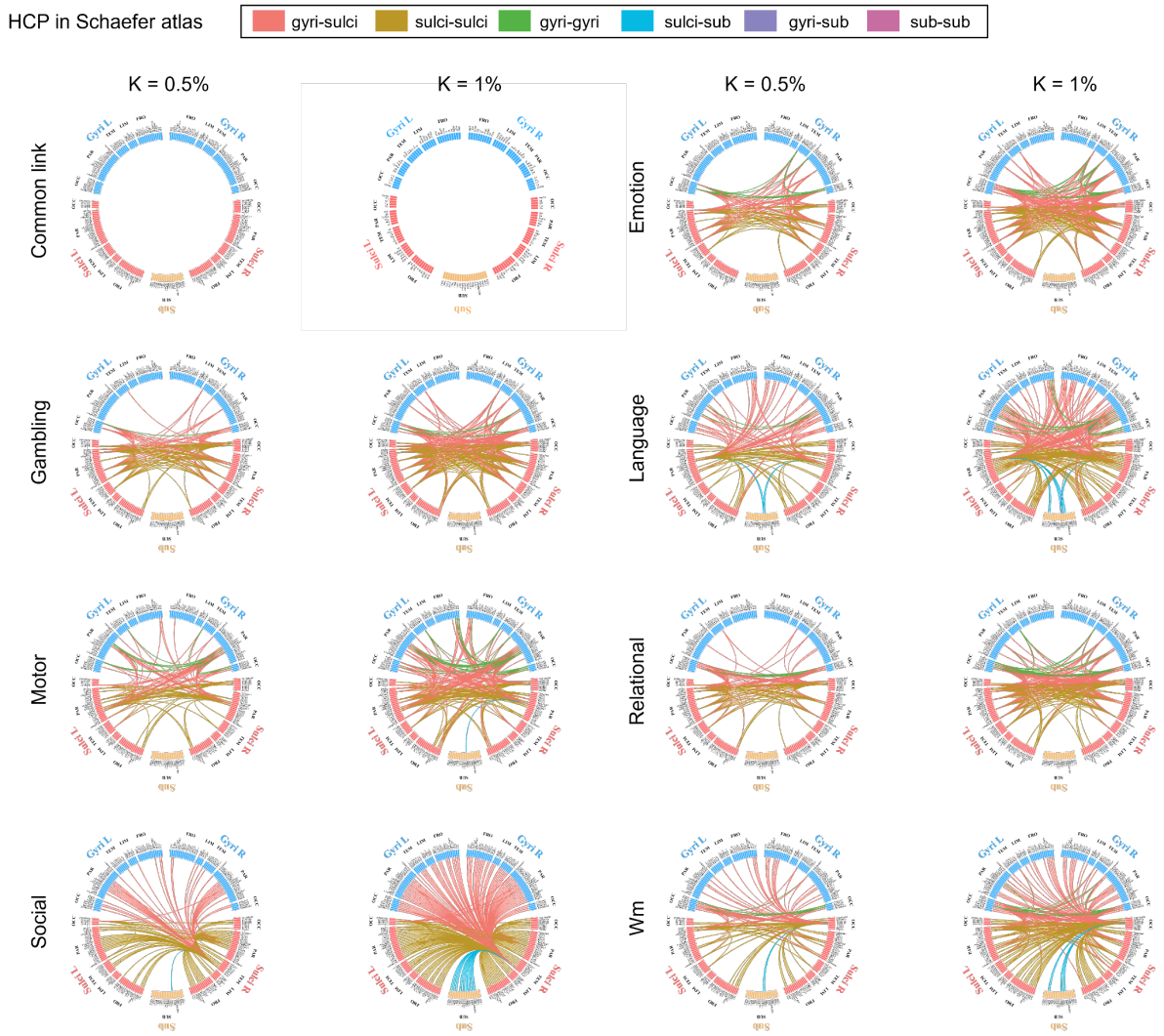

Fig. S24: Visualization of important connections in top 0.5 and 1 percent in HCP dataset in Schaefer atlas.

FIG. S25

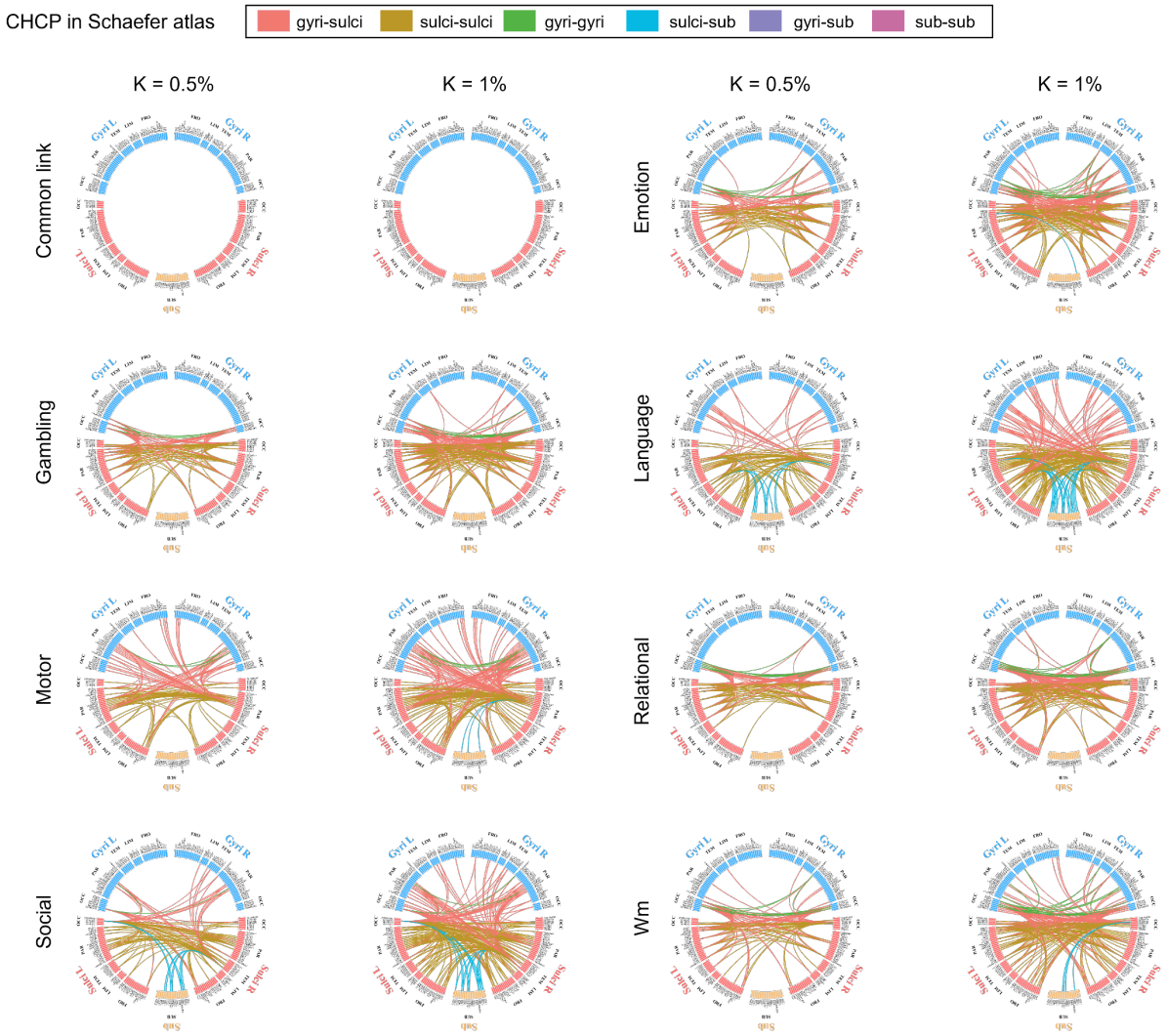

Fig. S25: Visualization of important connections in top 0.5 and 1 percent in CHCP dataset in Schaefer atlas.

FIG. S26

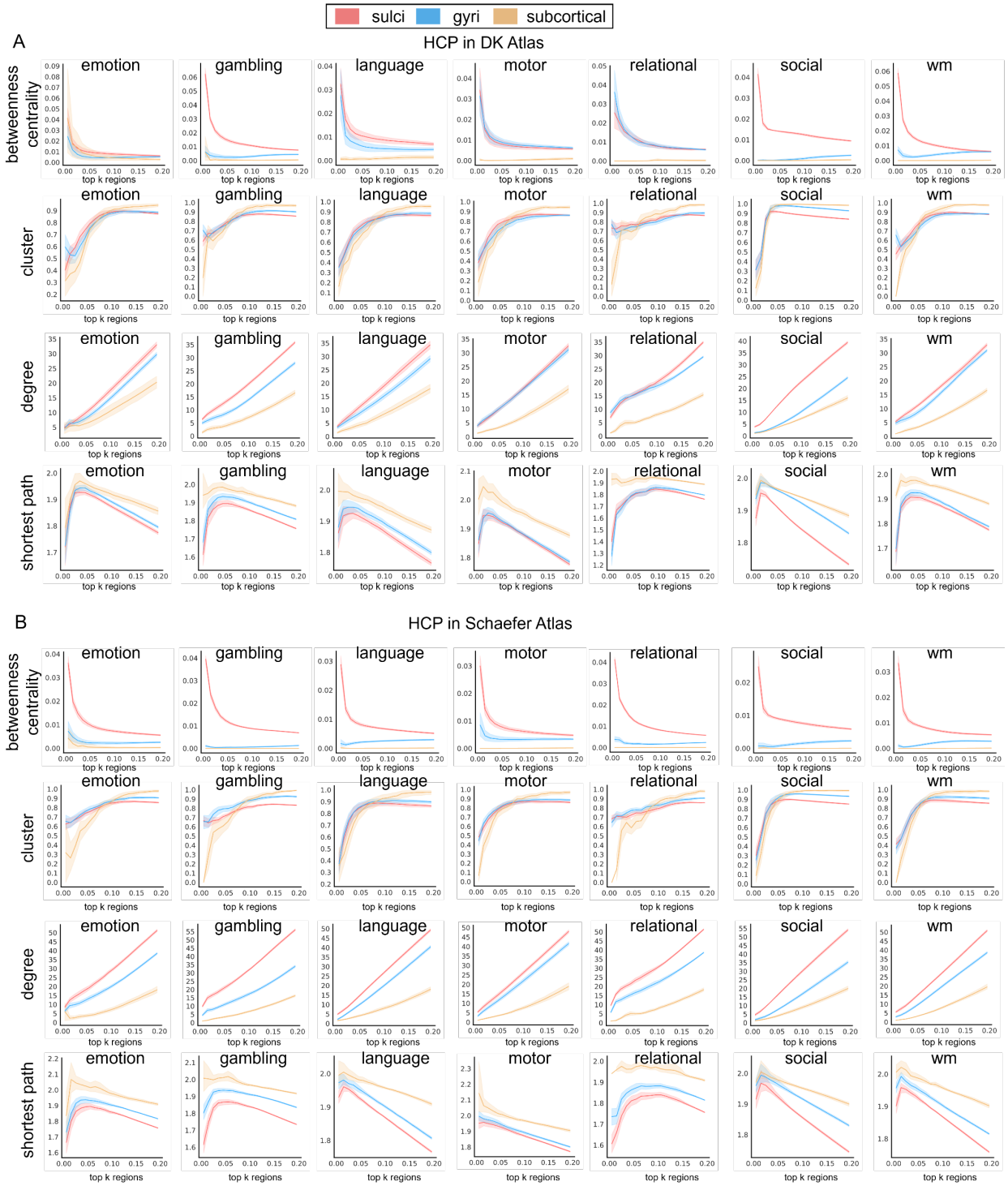

Fig. S26: Application for four graph theory in HCP DK/Schaefer atlas. We choose top 0.5percent to top 20 percent as threshold with a 0.1 percent threshold.

FIG. S27

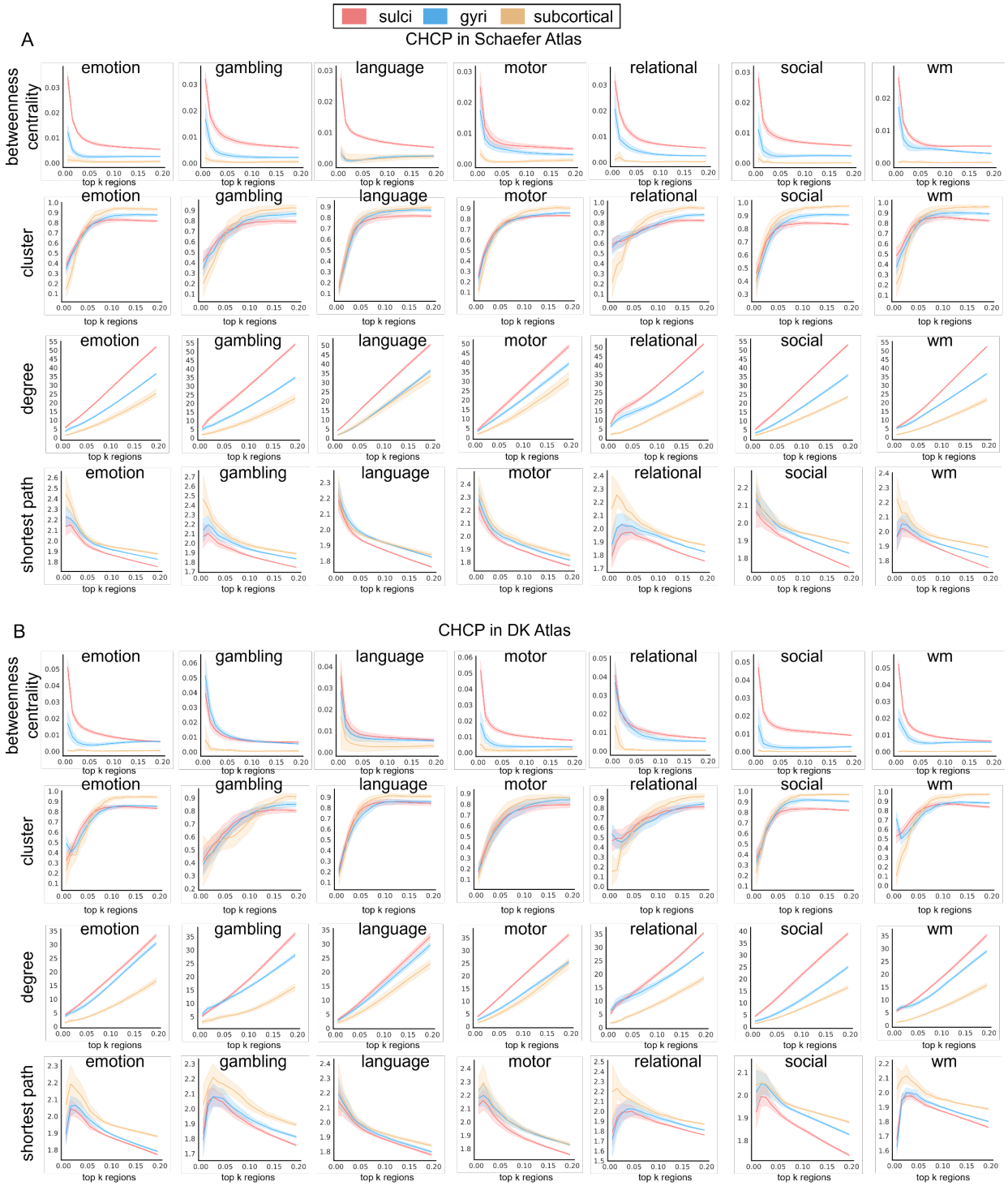

Fig. S27: Application for four graph theory in HCP DK/Schaefer atlas. We choose top 0.5percent to top 20 percent as threshold with a 0.1 percent threshold.

FIG. S28

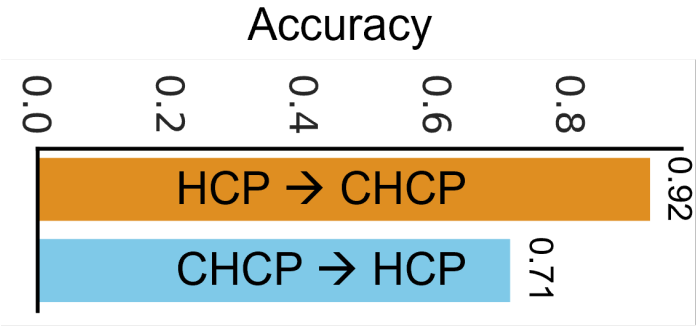

Fig. S28: Zero-parameter update cross-testing in Schaefer atlas.

Table S1

Model architecture in DK atlas

Layer	Input Shape	Connected Layer	Output Shape	Parameter
Input	[155, 155]	Patch embed	[1, 155, 768]	119040
Patch embed	[1,155, 768]	Position embed	[1, 156, 768]	119808
Position embed	[1, 156, 768]	Layer Norm	[1, 156, 768]	768
Norm1: Layer Norm	[1, 156, 768]	Norm1: Attention(q, k, v)	[1, 156, 2304]	1769472
Norm1: Attention(q, k, v)	[1, 156, 2304]	Norm1: Linear(q, k, v)	[1, 156, 768]	589824
Norm1: Linear(q, k, v)	[1, 156, 768]	Norm2: Layer Norm	[1, 156, 768]	119808
Norm2: Layer Norm	[1, 156, 768]	Norm2: MLP (fc1)	[1, 156, 3072]	2359296
Norm2: MLP (fc1)	[1, 156, 3072]	Norm2: MLP (fc2)	[1, 156, 768]	2359296
MLP (fc2)	[1, 156, 768]	Output	[7]	5383
One block: Norm1+Norm2 Total blocks: 12 Heads: 12				Total parameter: 85301767

Table S2.

Model architecture in Schaefer atlas

Layer	Input Shape	Connected Layer	Output Shape	Parameter
Input	[219, 219]	Patch embed	[1, 219, 768]	168192
Patch embed	[1, 219, 768]	Position embed	[1, 220, 768]	168960
Position embed	[1, 220, 768]	Layer Norm	[1, 220, 768]	768
Norm1: Layer Norm	[1, 220, 768]	Norm1: Attention(q, k, v)	[1, 220, 2304]	1769472
Norm1: Attention(q, k, v)	[1, 220, 2304]	Norm1: Linear(q, k, v)	[1, 220, 768]	589824
Norm1: Linear(q, k, v)	[1, 220, 768]	Norm2: Layer Norm	[1, 220, 768]	119808
Norm2: Layer Norm	[1, 220, 768]	Norm2: MLP (fc1)	[1, 156, 3072]	2359296
Norm2: MLP (fc1)	[1, 220, 3072]	Norm2: MLP (fc2)	[1, 220, 768]	2359296
MLP (fc2)	[1, 220, 768]	Output	[7]	5383
One block: Norm1+Norm2 Total blocks: 12 Heads: 12				Total parameter: 85400071

References and Notes

1. W. R. Uttal, *The new phrenology: The limits of localizing cognitive processes in the brain*. (The MIT press, 2001).
2. R. J. Joynt, Paul Pierre Broca: His contribution to the knowledge of aphasia. *Cortex* **1**, 206-213 (1964).
3. W. Penfield, E. Boldrey, Somatic motor and sensory representation in the cerebral cortex of man as studied by electrical stimulation. *Brain* **60**, 389-443 (1937).
4. K. Brodmann, *Vergleichende Lokalisationslehre der Grosshirnrinde in ihren Prinzipien dargestellt auf Grund des Zellenbaues*. (Barth, 1909).
5. L. R. Squire, J. T. Wixted, The cognitive neuroscience of human memory since HM. *Annual review of neuroscience* **34**, 259-288 (2011).
6. H. Klüver, P. C. Bucy, " Psychic blindness" and other symptoms following bilateral temporal lobectomy in Rhesus monkeys. *American Journal of Physiology*, (1937).
7. R. S. Desikan *et al.*, An automated labeling system for subdividing the human cerebral cortex on MRI scans into gyral based regions of interest. *Neuroimage* **31**, 968-980 (2006).
8. A. Schaefer *et al.*, Local-global parcellation of the human cerebral cortex from intrinsic functional connectivity MRI. *Cerebral cortex* **28**, 3095-3114 (2018).
9. K. Friston, Beyond phrenology: what can neuroimaging tell us about distributed circuitry? *Annual review of neuroscience* **25**, 221-250 (2002).
10. Y. Du *et al.*, NeuroMark: An automated and adaptive ICA based pipeline to identify reproducible fMRI markers of brain disorders. *NeuroImage: Clinical* **28**, 102375 (2020).
11. K. J. Friston, Functional and effective connectivity: a review. *Brain connectivity* **1**, 13-36 (2011).
12. K. J. Friston, Modalities, Modes, and Models in Functional Neuroimaging. **326**, 399-403 (2009).
13. J. Duncan, The multiple-demand (MD) system of the primate brain: mental programs for intelligent behaviour. *Trends in cognitive sciences* **14**, 172-179 (2010).
14. M. W. Cole, W. Schneider, The cognitive control network: Integrated cortical regions with dissociable functions. *Neuroimage* **37**, 343-360 (2007).
15. B. T. T. Yeo *et al.*, The organization of the human cerebral cortex estimated by intrinsic functional connectivity. *Journal of neurophysiology*, (2011).
16. M. Jiang *et al.*, Anatomy-guided spatio-temporal graph convolutional networks (AG-STGCNs) for modeling functional connectivity between gyri and sulci across multiple task domains. *IEEE Transactions on Neural Networks and Learning Systems*, (2022).
17. M. Schurz, L. Maliske, P. Kanske, Cross-network interactions in social cognition: A review of findings on task related brain activation and connectivity. *cortex* **130**, 142-157 (2020).
18. R. Jiang *et al.*, Task-induced brain connectivity promotes the detection of individual differences in brain-behavior relationships. *NeuroImage* **207**, 116370 (2020).
19. A. Segal *et al.*, Regional, circuit and network heterogeneity of brain abnormalities in psychiatric disorders. *Nature Neuroscience*, 1-17 (2023).
20. D. M. Barch *et al.*, Function in the human connectome: task-fMRI and individual differences in behavior. *Neuroimage* **80**, 169-189 (2013).
21. B. Biswal, F. Zerrin Yetkin, V. M. Haughton, J. S. Hyde, Functional connectivity in the motor cortex of resting human brain using echo‐planar MRI. *Magnetic resonance in medicine* **34**, 537-541 (1995).
22. P. Zaramella *et al.*, Brain Auditory Activation Measured by Near-Infrared Spectroscopy (NIRS) in Neonates. *Pediatric Research* **49**, 213-219 (2001).
23. J. Lv *et al.*, Sparse representation of whole-brain fMRI signals for identification of functional networks. *Medical image analysis* **20**, 112-134 (2015).
24. A. H. Andersen, D. M. Gash, M. J. Avison, Principal component analysis of the dynamic response measured by fMRI: a generalized linear systems framework. *Magnetic resonance imaging* **17**, 795-815 (1999).

25. M. J. McKeown *et al.*, Spatially independent activity patterns in functional MRI data during the Stroop color-naming task. *Proceedings of the National Academy of Sciences* **95**, 803-810 (1998).
26. D. Van De Ville, Y. Farouj, M. G. Preti, R. Liégeois, E. Amico, When makes you unique: Temporality of the human brain fingerprint. **7**, eabj0751 (2021).
27. A. Dosovitskiy *et al.*, An image is worth 16x16 words: Transformers for image recognition at scale. *arXiv preprint arXiv:2010.11929*, (2020).
28. H. Chefer, S. Gur, L. Wolf. pp. 782-791.
29. W. Welker, Why does cerebral cortex fissure and fold? A review of determinants of gyri and sulci. *Cerebral Cortex: comparative structure and evolution of Cerebral Cortex, Part II*, 3-136 (1990).
30. E. A. Miska *et al.*, Microarray analysis of microRNA expression in the developing mammalian brain. *Genome biology* **5**, 1-13 (2004).
31. D. P. Richman, R. M. Stewart, J. Hutchinson, V. S. Caviness Jr, Mechanical Model of Brain Convolutional Development: Pathologic and experimental data suggest a model based on differential growth within the cerebral cortex. *Science* **189**, 18-21 (1975).
32. B. Mota, S. Herculano-Houzel, How the cortex gets its folds: an inside-out, connectivity-driven model for the scaling of mammalian cortical folding. *Frontiers in neuroanatomy* **6**, 3 (2012).
33. D. C. v. Essen, A tension-based theory of morphogenesis and compact wiring in the central nervous system. *Nature* **385**, 313-318 (1997).
34. J. Nie *et al.*, Axonal fiber terminations concentrate on gyri. *Cerebral cortex* **22**, 2831-2839 (2012).
35. I. H. M. Smart, C. Dehay, P. Giroud, M. Berland, H. Kennedy, Unique morphological features of the proliferative zones and postmitotic compartments of the neural epithelium giving rise to striate and extrastriate cortex in the monkey. *Cerebral cortex* **12**, 37-53 (2002).
36. B. Fischl, A. M. Dale, Measuring the thickness of the human cerebral cortex from magnetic resonance images. *Proceedings of the National Academy of Sciences* **97**, 11050-11055 (2000).
37. V. A. Magnotta *et al.*, Quantitative in vivo measurement of gyrification in the human brain: changes associated with aging. *Cerebral Cortex* **9**, 151-160 (1999).
38. X. Jiang, T. Zhang, S. Zhang, K. M. Kendrick, T. Liu, Fundamental functional differences between gyri and sulci: implications for brain function, cognition, and behavior. *Psychoradiology* **1**, 23-41 (2021).
39. H. Liu *et al.*, The cerebral cortex is bisectionally segregated into two fundamentally different functional units of gyri and sulci. *Cerebral Cortex* **29**, 4238-4252 (2019).
40. F. Deng *et al.*, A functional model of cortical gyri and sulci. *Brain structure and function* **219**, 1473-1491 (2014).
41. R. Malach *et al.*, Object-related activity revealed by functional magnetic resonance imaging in human occipital cortex. *Proceedings of the National Academy of Sciences* **92**, 8135-8139 (1995).
42. K. Grill-Spector *et al.*, Differential processing of objects under various viewing conditions in the human lateral occipital complex. *Neuron* **24**, 187-203 (1999).
43. Z. Kourtzi, N. Kanwisher, Representation of perceived object shape by the human lateral occipital complex. *Science* **293**, 1506-1509 (2001).
44. N. Kanwisher, J. McDermott, M. M. Chun, The fusiform face area: a module in human extrastriate cortex specialized for face perception. *Journal of neuroscience* **17**, 4302-4311 (1997).
45. N. Kanwisher, G. Yovel, The fusiform face area: a cortical region specialized for the perception of faces. *Philosophical Transactions of the Royal Society B: Biological Sciences* **361**, 2109-2128 (2006).
46. A. Mechelli, G. W. Humphreys, K. Mayall, A. Olson, C. J. Price, Differential effects of word length and visual contrast in the fusiform and lingual gyri during. *Proceedings of the Royal Society of London. Series B: Biological Sciences* **267**, 1909-1913 (2000).
47. D. M. Wolpert, S. J. Goodbody, M. Husain, Maintaining internal representations: the role of the human superior parietal lobe. *Nature neuroscience* **1**, 529-533 (1998).
48. C. A. Hynes, A. A. Baird, S. T. Grafton, Differential role of the orbital frontal lobe in emotional versus cognitive perspective-taking. *Neuropsychologia* **44**, 374-383 (2006).

49. A. Fornito *et al.*, Individual differences in anterior cingulate/paracingulate morphology are related to executive functions in healthy males. *Cerebral cortex* **14**, 424-431 (2004).
50. A. Cachia *et al.*, How interindividual differences in brain anatomy shape reading accuracy. *Brain Structure and Function* **223**, 701-712 (2018).
51. L. W. Swanson, G. D. Petrovich, What is the amygdala? *Trends in neurosciences* **21**, 323-331 (1998).
52. P. H. Janak, K. M. Tye, From circuits to behaviour in the amygdala. *Nature* **517**, 284-292 (2015).
53. J. E. Ledoux, Emotion and the amygdala. (1992).
54. J. LeDoux, The amygdala. *Current biology* **17**, R868-R874 (2007).
55. G. Z. Tau, B. S. Peterson, Normal development of brain circuits. *Neuropsychopharmacology* **35**, 147-168 (2010).
56. M. A. Sommer, R. H. Wurtz, Brain circuits for the internal monitoring of movements. *Annu. Rev. Neurosci.* **31**, 317-338 (2008).
57. D. C. Van Essen *et al.*, The WU-Minn human connectome project: an overview. *Neuroimage* **80**, 62-79 (2013).
58. M. F. Glasser *et al.*, The minimal preprocessing pipelines for the Human Connectome Project. *Neuroimage* **80**, 105-124 (2013).
59. J. S. Elam *et al.*, The human connectome project: a retrospective. *NeuroImage* **244**, 118543 (2021).
60. D. C. Van Essen *et al.*, The Human Connectome Project: a data acquisition perspective. *Neuroimage* **62**, 2222-2231 (2012).
61. J. Ge *et al.*, Increasing diversity in connectomics with the Chinese Human Connectome Project. *Nature Neuroscience* **26**, 163-172 (2023).
62. N. Vogt, The Chinese Human Connectome Project. *Nature Methods* **20**, 177-177 (2023).
63. M. F. Glasser *et al.*, The minimal preprocessing pipelines for the Human Connectome Project. **80**, 105-124 (2013).
64. B. Fischl, M. I. Sereno, A. M. Dale, Cortical surface-based analysis: II: inflation, flattening, and a surface-based coordinate system. *Neuroimage* **9**, 195-207 (1999).
65. S. Yang *et al.*, Temporal variability of cortical gyral-sulcal resting state functional activity correlates with fluid intelligence. *Frontiers in neural circuits* **13**, 36 (2019).
66. T. Miyato, A. M. Dai, I. Goodfellow, Adversarial training methods for semi-supervised text classification. *arXiv preprint arXiv:1605.07725*, (2016).
67. I. J. Goodfellow, J. Shlens, C. Szegedy, Explaining and harnessing adversarial examples. *arXiv preprint arXiv:1412.6572*, (2014).
68. T. Zhang, Z. Zhu. (PMLR), pp. 7502-7511.

Acknowledgments: Data were provided in part by the Chinese Human Connectome Project (CHCP, PI: Jia-Hong Gao) funded by the Beijing Municipal Science & Technology Commission, Chinese Institute for Brain Research (Beijing), National Natural Science Foundation of China, and the Ministry of Science and Technology of China.

Funding: This study was partly supported by the National Natural Science Foundation of China (62276050, 61976045).

Author contributions:

Conceptualization: Zifan Wang, Xi Jiang

Methodology: Zifan Wang, Yuzhong Chen, Wei Mao, Zhenxiang Xiao

Visualization: Zifan Wang, Xi Jiang

Funding acquisition: Xi Jiang

Project administration: Xi Jiang

Data curation: Zifan Wang, Guannan Cao, Zhenxiang Xiao

Supervision: Xi Jiang, Alan C Evans, Paule-J Toussaint

Writing – original draft: Zifan Wang

Writing – review & editing: Xi Jiang, Alan C Evans, Paule-J Toussaint

Competing interestings: Authors declare that they have no competing interestings.

Data and materials availability: All data are available in the main text or the supplementary materials. The HCP dataset is available in https://www.humanconnectome.org/, CHCP dataset is available in https://www.Chinese-HCP.cn. See XiJiangLabUESTC/Fingerprint: This is the code for 'Multi-task machine learning reveals the neuroanatomy fingerprint of mental processing' (github.com) for code.

Supplementary Materials

Materials and Methods

Supplementary Text

Figs. S1 to S28

Tables S1 to S2

References *(1–68)*